Stabilization of Complementarity Systems via Contact-Aware Controllers

Alp Aydinoglu, *Graduate Student Member, IEEE*, Philip Sieg, Victor M. Preciado, and Michael Posa, *Member, IEEE*

***Abstract*—We propose a control framework, which can utilize tactile information by exploiting the complementarity structure of contact dynamics. Since many robotic tasks, like manipulation and locomotion, are fundamentally based in making and breaking contact with the environment, state-of-the-art control policies struggle to deal with the hybrid nature of multicontact motion. Such controllers often rely heavily upon heuristics or, due to the combinatorial structure in the dynamics, are unsuitable for real-time control. Principled deployment of tactile sensors offers a promising mechanism for stable and robust control, but modern approaches often use this data in an ad hoc manner, for instance to guide guarded moves. This framework can close the loop on tactile sensors and it is noncombinatorial, enabling optimization algorithms to automatically synthesize provably stable control policies. We demonstrate this approach on multiple numerical examples, including quasi-static friction problems and a high dimensional problem with 10 contacts. We also validate our results on an experimental setup and show the effectiveness of the proposed method on an underactuated multicontact system.**

***Index Terms*—Bilinear matrix inequalities (BMIs), force control, optimization-based control, tactile feedback.**

I. Introduction

In RECENT years, robotic automation has excelled in dealing with repetitive tasks in static and structured environments. On the other hand, to achieve the promise of the field, robots must perform efficiently in complex, unstructured environments that involve physical interaction between the robot and the environment itself, which has been an ongoing research direction for many years [1], [2]. Furthermore, as compared with traditional motion planning problems, tasks like dexterous manipulation and legged locomotion fundamentally require intentionally initiating contact with the environment to achieve a positive result. To enable stable, and robust motion, it is critically important to design policies that explicitly consider the interaction between robot and environment.

Contact, however, is hybrid or multimodal in nature, capturing the effect of stick-slip transitions or making and breaking contact. Standard approaches to control often match the hybrid dynamics with a hybrid or switching controller, where one policy is associated with each mode. However, precise identification of the hybrid events is difficult in practice, and switching controllers can be brittle, particularly local to the switching surface, or require significant hand-tuning. Model predictive control, closely related to this work, is one approach that has been regularly applied to control through contact, with notable successes. Due to the computational complexity of hybrid model predictive control, most of these approaches have not been demonstrated to work in real-time for dynamic problems [3], [4]. Methods that work in real-time must either approximate the hybrid dynamics (e.g., [5]), or limit online control to a known mode sequence [6]. Most of these approaches do not provide stability guarantees. Methods that provide guarantees [7] require significant online computation time and have not been shown to work in real-time applications.

While prior work has explored computational synthesis of nonswitching feedback policies [8], it does not incorporate tactile sensing, and there are clear structural limits to smooth, nonswitching, state-based control. Here, we focus on offline synthesis of a stabilizing feedback policy, eliminating the need for intensive online calculations.

The need for contact-aware control is driven, in part, by recent advances in tactile sensing (e.g., [9]–[13] and others). Given these advances, there has been ongoing research to design control policies using tactile feedback for tasks that require making and breaking contact. However, these approaches are largely based on static assumptions, for instance with guarded moves [14], or rely upon switching controllers (e.g., [15], [16]). Other recent methods incorporate tactile sensors within deep learning frameworks, though they offer no guarantees on performance or stability [17], [18].

In this work, we present an optimization-based numerical approach for designing control policies that use feedback on the contact forces. The control policy combines regular state feedback with tactile feedback in order to provably stabilize systems with possibly nonunique solutions. Our controller structure is noncombinatorial in nature and avoids enumerating the exponential number of potential hybrid modes that might arise

Manuscript received June 28, 2021; accepted September 13, 2021. Date of publication November 15, 2021; date of current version June 7, 2022. This work was supported by the National Science Foundation under Grant CMMI-1830218. This article was recommended for publication by Associate Editor O. Stasse and Editor E. Yoshida upon evaluation of the reviewers' comments. *(Corresponding author: Alp Aydinoglu.)*

Alp Aydinoglu, Philip Sieg, and Michael Posa are with the General Robotics, Automation, Sensing, and Perception (GRASP) Laboratory, University of Pennsylvania, Philadelphia, PA 19104 USA (e-mail: alpayd@seas.upenn.edu; philsieg@seas.upenn.edu; posa@seas.upenn.edu).

Victor M. Preciado is with the Department of Electrical, and Systems Engineering, University of Pennsylvania, Philadelphia, PA 19104 USA (e-mail: victormpreciado@gmail.com).

This article has supplementary material provided by the authors and color versions of one or more figures available at https://doi.org/10.1109/TRO.2021.3120931.

Digital Object Identifier 10.1109/TRO.2021.3120931

from contact. More precisely, the contributions of each contact are additive, rather than combinatorial. Inspired by both prior work [8] and [19], we synthesize and verify a corresponding nonsmooth, piecewise quadratic Lyapunov function. Additionally, we are able to explicitly define sparsity patterns allowing us to design controllers for systems, where the full state information might be lacking, such as when the state of an object is unknown but tactile information is available.

The primary contribution of this article is an algorithm for synthesis of a control policy, utilizing state, and force feedback, which is provably stabilizing even during contact mode transitions for systems with possibly nonunique solutions. To achieve this, we choose a structure for controller and Lyapunov function designed specifically to leverage the complementarity structure of contact. While verification can be posed as a convex optimization problem, control synthesis is inherently harder. This problem is formulated and solved as a bilinear matrix inequality (BMI).

A preliminary version of this article was presented at the International Conference on Robotics and Automation [20]. In this work, extensions are as follows.

1) The results are extended to a significantly broader class of systems.
   a) The P-matrix assumption (see Section II) is removed, which enables design for systems with nonunique solutions (see Section III).
   b) Models where there is a coupling between the contact force and the control loop, including friction models are discussed (see Section III).
   c) Stability analysis (see Section IV, Theorem 12) for this broader class of systems is presented.
2) Better approximations for the sets used in S-procedure [see Section V, (14)] are introduced.
3) A polynomial optimization program [see Section V, (27)] that can describe the nonunique solution sets of linear complementarity problems (LCPs) is introduced.
4) Four new examples are presented. Three of them are quasi-static friction models with nonunique contact forces. The fourth is a high dimensional example with eight states and ten contacts.
5) Results are verified on an experimental setup, and the effectiveness of the proposed method is shown on the task of stabilizing a cart-pole with soft walls.

II. Background

We first introduce the definitions and notation used throughout this work. For a positive integer l, $\bar{l}$ denotes the set $\{1, 2, \ldots, l\}$. Given a matrix $M \in \mathbb{R}^{k\times l}$ and two subsets $I \subseteq \bar{k}$ and $J \subseteq \bar{l}$, we define $M_{IJ} = (m_{ij})_{i\in I, j\in J}$. For two vectors $a \in \mathbb{R}^m$ and $b \in \mathbb{R}^m$, the notation $0 \leq a \perp b \geq 0$ is used to denote that $a \geq 0,\ b \geq 0,\ a^T b = 0$. The collection of all absolutely continuous functions on a closed interval $[\alpha, \beta]$ is denoted as $AC([\alpha, \beta])$. The indeterminates are denoted with bold vectors, e.g., $\boldsymbol{x}$.

A. Linear Complementarity Systems (LCSs)

A standard approach to modeling robotic systems is through the framework of rigid-body systems with contacts. The continuous time dynamics can be modeled by manipulator equations

$$M(q)\dot{v} + C(q, v) = Bu + J(q)^T \lambda \tag{1}$$

where q represents the generalized coordinates, v represents the generalized velocities, $\lambda \in \mathbb{R}^m$ represents the contact forces, $M(q)$ is the inertia matrix, $C(q, v)$ represents the combined Coriolis, centrifugal, and gravitational terms, B maps the control inputs $u \in \mathbb{R}^k$ into joint coordinates and $J(q)$ is the projection matrix (typically the contact Jacobian).

The model (1) is a hybrid dynamical system [21], [22], where the number of modes scales exponentially with m, which arises from distinct combinations of contacts. One approach to contact dynamics describes the forces using the complementarity framework, where the generalized coordinates q, velocities v, and contact forces λ satisfy a set of complementarity constraints

$$\lambda \geq 0,\ \phi(q, v, \lambda) \geq 0,\ \phi(q, v, \lambda)^T \lambda = 0 \tag{2}$$

where the function $\phi : \mathbb{R}^p \times \mathbb{R}^m \to \mathbb{R}^m$ relates the position and velocity of the robot with contact force ([23]–[26] for more details). The complementarity framework is widespread within the robotics community and has been commonly used to simulate contact dynamics [27], [28], leveraged in trajectory optimization [29], stability analysis [30], [31], adaptive control [32], passivity-based control [33], [34], observer design [35], trajectory tracking [36], [37], and feedback control [38]–[40] of rigid-body systems with contacts.

The local behavior of (1) with the constraints (2) can be captured by LCSs [41], [42]. A LCS is characterized by: $\bar{A} \in \mathbb{R}^{n_x\times n_x},\ B \in \mathbb{R}^{n_x\times n_k},\ \bar{D} \in \mathbb{R}^{n_x\times m},\ a \in \mathbb{R}^{n_x},\ \bar{E} \in \mathbb{R}^{m\times n_x}$, $\bar{F} \in \mathbb{R}^{m\times m}, H \in \mathbb{R}^{m\times n_k}, c \in \mathbb{R}^m$ in the following way:

Definition 1: (LCS). A LCS describes the evolution of two time-dependent trajectories $\bar{x}(t) \in \mathbb{R}^{n_x}$ and $\lambda(t) \in \mathbb{R}^m$ for a given $u(t) \in \mathbb{R}^{n_k}$ and $\bar{x}(0)$ such that

$$\begin{aligned} \dot{\bar{x}} &= \bar{A}\bar{x} + Bu + \bar{D}\lambda + a \\ 0 \leq \lambda &\perp \bar{E}\bar{x} + \bar{F}\lambda + Hu + c \geq 0 \end{aligned} \tag{3}$$

where $\bar{A}$ determines the autonomous dynamics of the state vector $\bar{x}$, B models the effect of the input on the state, $\bar{D}$ describes the effect of the contact forces on the state and a models the constant forces acting on the state.

The matrices $\bar{E}, \bar{F}, H$[1] and the vector c capture the relationship between the contact force λ, the state vector $\bar{x}$ and the input u. Note that the contact forces λ are always nonnegative, which holds for basic model of normal force and slack variables are typically used to represent sign-indefinite frictional forces. (3) implies that either $\lambda = 0$ or $\bar{E}\bar{x} + \bar{F}\lambda + Hu + c = 0$, encoding the multimodal dynamics of contact. Due to this complementarity structure, an LCS is a compact representation, as the variables and constraints scale linearly with m, rather than with the potential 2^m hybrid modes [19], [43].

[1]Even though the contact force λ does not depend on the input u in (2), local approximations of (1) and (2) can lead to models, where the contact force depends on the input under the quasi-static assumption, e.g., [23], when v depends on the input u and $x = q$. An important example where the contact force depends on the input is quasi-static friction models (see Sections VI-D, VI-E, VI-F) and this affect is captured by the Hu term in the LCS.

B. Linear Complementarity Problem (LCP)

A LCS is an ordinary differential equation coupled with a variable that is the solution of a LCP. Since LCPs play an important role in understanding and analyzing the LCS, some definitions and results from the theory of LCPs are summarized [44].

Definition 2: (LCP). Given $F \in \mathbb{R}^{m\times m}$ and a vector $w \in \mathbb{R}^m$, the LCP(w, F) is the following mathematical program:

$$\begin{aligned} &\text{find} && \lambda \in \mathbb{R}^m \\ &\text{subject to} && 0 \le \lambda \perp F\lambda + w \ge 0. \end{aligned} \tag{4}$$

For a given F and w, the LCP may have multiple solutions or none at all. Hence, the solution set of the LCP(w, F) is

$$\text{SOL}(w, F) = \{\lambda : 0 \le \lambda \perp F\lambda + w \ge 0\}.$$

In this work, we will consider LCPs, where SOL(w, F) can have more than one element for a given F and w. As a special case of this, we mention a particular class of LCP's that are guaranteed to have unique solutions.

Definition 3: (P-Matrix) A matrix $F \in \mathbb{R}^{m\times m}$ is a P-matrix, if the determinants of all of its principal submatrices are positive; that is, $\det(F_{\alpha\alpha}) > 0$ for all $\alpha \subseteq \{1, \ldots, m\}$.

If F is a P-matrix, then the solution set SOL(w, F) is a singleton for any $w \in \mathbb{R}^m$ [45]. If the unique element of SOL(w, F) is $\psi(w)$, then it is a piecewise linear function in $w \in \mathbb{R}^m$, hence is Lipschitz continuous and directionally differentiable.

If $\bar{F}$ is a P-matrix, one can represent an LCS in a more compact manner. The LCS in (3) is equivalent to the dynamical system

$$\dot{\bar{x}} = \bar{A}\bar{x} + Bu + \bar{D}\lambda(\bar{x}, u) \tag{5}$$

where $\lambda(\bar{x}, u)$ corresponds to the unique element of SOL$(\bar{E}\bar{x} + Hu + c, \bar{F})$ for every state vector $\bar{x}$. Notice that (5) is only a an alternative representation of (3) and still has the same structure as the LCS.

C. Sum-of-Squares

In this work [see Section V, (27)], describing the nonunique solution sets of LCP's is posed as a question of nonnegativity of polynomials on basic semialgebraic sets. Toward this direction, sum-of-squares (SOS) optimization is used.

A multivariate polynomial $p(x)$ is a SOS if there exist polynomials $q_i(x)$ such that

$$p(x) = \sum_i q_i^2(x).$$

The existence of a SOS decomposition of a polynomial can be decided by solving a semidefinite programming (SDP) feasibility problem [46], which is a convex optimization problem. We represent the semialgebraic conditions using the S-procedure technique [47], [48]. For example, to show that [49]

$$f(x) \ge 0, \quad \forall x \in \{z : g(z) \ge 0, h(z) = 0\}$$

it is sufficient to find polynomials $\sigma_1(x), \sigma_2(x), q(x)$ s.t.

$$\sigma_1(x)f(x) - \sigma_2(x)g(x) - q(x)h(x) \ge 0$$
$$\sigma_1(x) - 1 \ge 0$$
$$\sigma_2(x) \ge 0. \tag{6}$$

If constraints are in the form of (6) and the objective function is linear in the coefficients of any unknown/free polynomials, then the optimization problem can be represented as a SDP using the SOS relaxation.

III. LCS With Tactile Feedback

In this section, we present a tactile feedback controller, where the input is dependent both on the state and the contact force $(u = u(x, \lambda))$, unlike the common approach of designing controllers only using the state feedback, $(u = u(x))$. The section concludes with a description of complementarity models with such tactile feedback controllers.

A. Tactile Feedback and Related Complementarity Models

We introduce the tactile feedback controller

$$u(\bar{x}, \lambda) \;=\; K\bar{x} + L\lambda \tag{7}$$

where $K \in \mathbb{R}^{n_k\times n_x}$ and $L \in \mathbb{R}^{n_k\times m}$. Using this control law, (3) can be transformed into the following LCS:

$$\begin{aligned} \dot{x} &= Ax + D\lambda + a \\ 0 \le \lambda &\perp Ex + F\lambda + c \ge 0 \end{aligned} \tag{8}$$

where $A \in \mathbb{R}^{n\times n}$, $D \in \mathbb{R}^{n\times m}$, $a \in \mathbb{R}^n$, $E \in \mathbb{R}^{m\times n}$, $F \in \mathbb{R}^{m\times m}$, $c \in \mathbb{R}^m$.

If the contact force does not depend on the input $(H = 0)$, then application of the control law (7) trivially produces (8) with $A = \bar{A} + BK$, $D = \bar{D} + BL$, $E = \bar{E}$, and $F = \bar{F}$. In this case, note that $x = \bar{x}$ and $n = n_x$.

Next, consider the case where the contact force depends on the input $(H \ne 0)$. Since the input $u = u(\bar{x}, \lambda)$ similarly depends on the contact force, this introduces an algebraic loop. One might attempt to resolve this loop by simultaneously solving for both u and λ, leading to the closed-loop LCS

$$\dot{x} = (\bar{A} + BK)x + (\bar{D} + BL)\lambda + a$$
$$0 \le \lambda \perp Ex + F\lambda + c \ge 0$$

where $x = \bar{x}$, $E = \bar{E} + HK$, and $F = \bar{F} + HL$. Observe that the matrix F depends on the choice of the contact gain matrix L. Due to this dependency, the cardinality of the solution set SOL$(Ex + c, F)$ for a given x might change depending on the value of L. This is illustrated via an example.

Example 4: Consider the complementarity constraint

$$0 \le \lambda \perp x + u + \lambda \ge 0$$

where $x, u, \lambda \in \mathbb{R}$. If u is independent of λ, observe that SOL$(x + u, F)$ is a singleton for all pairs (x, u) since $F = [1]$ is a P-matrix. In this case, the contact force $\lambda_o(x, u)$ is equal to

$$\lambda_o(x, u) = \max\{0, -x - u\}.$$

However, for some choices of force-dependent inputs, this is no longer the case. From $u = L\lambda$, it follows that $F = [1 + L]$. For the case $L = -1$, the LCP for the closed-loop system is

$$0 \le \lambda \perp x \ge 0.$$

The solution set is then

$$\mathrm{SOL}(x, F=0) = \begin{cases} \{0\} & \text{if} \quad x > 0 \\ [0, \infty) & \text{if} \quad x = 0 \\ \emptyset & \text{if} \quad x < 0. \end{cases}$$

There are infinitely many solutions for $x = 0$ and no solutions for $x < 0$.

Furthermore, resolving the algebraic loop by solving simultaneously for the contact force and the input is not physically realistic, since control policies can not instantaneously respond to tactile measurements. As illustrated in Example 4, it is also mathematically problematic. Therefore, we will use the standard approach of modeling delay. Specifically, the following low-pass filter model captures the input delay

$$\dot{\tau} = \kappa(u - \tau) \tag{9}$$

where $\kappa \in \mathbb{R}^+$ is the rate parameter. Using the low-pass filter model, we obtain the LCS

$$\begin{aligned} \dot{\bar{x}} &= \bar{A}\bar{x} + B\tau + \bar{D}\lambda + a \\ \dot{\tau} &= \kappa(u - \tau) \\ 0 \leq \lambda \perp \bar{E}\bar{x} + F\lambda + H\tau + c &\geq 0. \end{aligned} \tag{10}$$

Observe that the LCS model in (10) has the same form with (8) with the input (7)

$$\begin{aligned} \dot{x} &= \begin{bmatrix} \bar{A} & B \\ \kappa K & -\kappa I \end{bmatrix} x +, \begin{bmatrix} \bar{D} \\ \kappa L \end{bmatrix} \lambda + \begin{bmatrix} a \\ 0 \end{bmatrix} \\ 0 \leq \lambda &\perp \begin{bmatrix} \bar{E} & H \end{bmatrix} x + F\lambda + c \geq 0 \end{aligned}$$

where $x = \begin{bmatrix} \bar{x}^T & \tau^T \end{bmatrix}^T$. Observe that the delay decouples u and λ so the matrix F does not depend on the contact gain matrix L. Notice that the state is augmented ($n > n_x$) to obtain (8). Alternatively, one could add delay to the sensor dynamics

$$\dot{\tau}_s = \kappa_s(\lambda - \tau_s).$$

While this approach would similarly resolve the algebraic loop, in this work, we found out that modeling input delay produced better numerical results when combined with the algorithmic approach in Section V.

Using the control format in (7), for notational compactness, we will now exclusively consider closed-loop LCS in the form of (8). As a result of filtering, the matrix F will be independent of the tactile feedback gain L.

B. Solution Concept

We introduce a solution concept for complementarity systems (1) and (8) similar to ([50], Definition 3.6).

Definition 5: A pair of functions $(x(t), \lambda(t))$ is a solution of the complementarity system

$$\begin{aligned} \dot{x} &= f(x, \lambda) \\ 0 \leq \lambda &\perp \Phi(x, \lambda) \geq 0 \end{aligned}$$

where $f : \mathbb{R}^n \times \mathbb{R}^m \to \mathbb{R}^n$ and $\Phi : \mathbb{R}^n \times \mathbb{R}^m \to \mathbb{R}^m$ with the initial condition $x(0) = x_0$ if

$$x(t) \in AC([0, T]),\ \forall\, T \geq 0$$

$$\dot{x}(t) = f(x(t), \lambda(t)) \text{ for almost all } t \in \mathbb{R}^+$$

$$0 \leq \lambda(t) \perp \Phi(x(t), \lambda(t)) \geq 0 \text{ for almost all } t \in \mathbb{R}^+$$

$$\lambda(t) \text{ is almost everywhere differentiable.}$$

It is important to note that we restrict ourselves to complementarity systems, where the state, $x(t)$, is absolutely continuous which is well-studied in the literature ([34], [51], [52]). The models considered in this work have no jumps (e.g., impact). Observe that $\lambda(t)$ can be discontinuous and it is assumed that $\lambda(t)$ is almost everywhere differentiable moving forward. Consider the following proposition by Camlibel *et al.* [53].

Proposition 6: For every x_0, the LCS (8) has a unique C^1 (hence absolutely continuous) trajectory $x(t)$ defined for all $t \geq 0$ if and only if the set $D\mathrm{SOL}(Ex + c, F)$ is a singleton for every $x \in \mathbb{R}^n$.

Throughout this work, focus is on LCS models where $\bar{D}\mathrm{SOL}(Ex + c, F)$ is a singleton. Note that unlike $x(t)$, the trajectory $\lambda(t)$ is not necessarily unique which is observed in friction models (see Section VI). Recent results indicate that it may, ultimately, be possible to eliminate this assumption on $\bar{D}\mathrm{SOL}(Ex + c, F)$ [52], [54], though such exploration is outside the scope of this work.

In Sections IV and V, this structure is leveraged to similarly ensure that $L\mathrm{SOL}(Ex + c, F)$ is a singleton for all x. Since we consider models such that $\bar{D}\mathrm{SOL}(Ex + c, F)$ is a singleton and F is independent of the controller (see Section III), the condition that $L\mathrm{SOL}(Ex + c, F)$ is a singleton suffices to ensure that $D\mathrm{SOL}(Ex + c, F)$ is also a singleton. The trajectories of the closed-loop system (8) remain absolutely continuous as long as $L\mathrm{SOL}(Ex + c, F)$ is a singleton for all x (following Proposition 6).

Moving forward, denote $\mathcal{S}(t_0, x_0)$ as the set of all trajectories $x(t)$, with $t \geq t_0$, such that $x(0) = x_0$. The dependency on the LCS parameters is suppressed for ease of notation. Observe that $S(t_0, x_0)$ is also a singleton following Proposition 6 if $D\mathrm{SOL}(Ex + c, F)$ is a singleton for every x.

IV. Stabilization of the LCS

In this section, conditions for stabilization using nonsmooth monontonic Lyapunov functions and contact-aware controllers are constructed.

Notions of stability from [55] are adopted. If F is a P-matrix, these are equivalent to the notions of stability for differential equations, where the right-hand side is Lipschitz continuous, though possibly nonsmooth [53], [56].

Definition 7: The equilibrium x_e of LCS (8) is

1) stable in the sense of Lyapunov if, given any $\epsilon > 0$, there exists $\delta > 0$ such that

$$||x_e - x_0|| < \delta \Rightarrow ||x(t) - x_e|| < \epsilon\ \forall t \geq 0$$

for any x_0 and $x(t) \in \mathcal{S}(0, x_0)$.

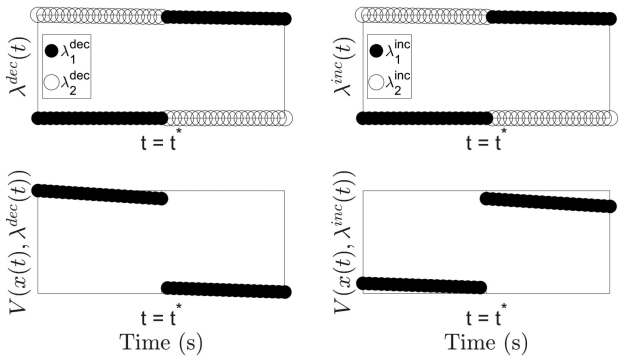

Fig. 1. Two different solutions for the Lyapunov function. For the solution λ^{dec}, λ_1^{dec} and λ_2^{dec} represent the first and second elements of the solution vector, respectively, (similarly for λ^{inc}).

2) asymptotically stable if it is stable and $\delta > 0$ exists s.t.

$$||x_e - x_0|| < \delta \Rightarrow \lim_{t\to\infty} x(t) = x_e$$

for any x_0 and $x(t) \in \mathcal{S}(0, x_0)$.

A. Nonsmooth Lyapunov Function

In Lyapunov-based analysis and synthesis methods, one desires to search over a wide class of functions. Here, piecewise quadratic Lyapunov functions are considered. They are more expressive than a Lyapunov function common to all modes (as was used in [8]), which makes it a more powerful choice than a single quadratic Lyapunov function [57]. Toward this direction, consider a variant of the Lyapunov function introduced in [53]

$$V(x,\lambda) = x^T P x + 2x^T Q\lambda + \lambda^T R\lambda + p^T x + r^T\lambda + z \tag{11}$$

where $P \in \mathbb{R}^{n\times n}$, $Q \in \mathbb{R}^{n\times m}$, $R \in \mathbb{R}^{m\times m}$, $p \in \mathbb{R}^n$, $r \in \mathbb{R}^m$, and $z \in \mathbb{R}$. The Lyapunov function (11) is quadratic in terms of the pair (x, λ). If F is a P-matrix, it is piecewise quadratic in x since $\lambda = \lambda(x)$ is a piecewise affine function. For example, if all contact forces are inactive, $\lambda = 0$, then $V(x, \lambda(x)) = x^T P x + p^T x + z$. Even though V is nonsmooth, it is locally Lipschitz continuous with respect to x if F is a P-matrix [53].

If $\text{SOL}(Ex + c, F)$ is not a singleton then $\lambda(t)$ can be discontinuous in t due to the multivalued nature of $\text{SOL}(Ex(t) + c, F)$. Similarly, $V(x(t), \lambda(t))$ can be discontinuous due to the terms $Q\text{SOL}(Ex(t) + c, F)$, $\text{SOL}(Ex(t) + c, F)^T R\text{SOL}(Ex(t) + c, F)$ and $r^T\text{SOL}(Ex(t) + c, F)$. Next, it is shown that without appropriate restrictions, these discontinuities imply that such functions V cannot be valid monotonic Lyapunov functions.

Example 8: Consider the LCS

$$\dot{x} = -x + \lambda_1 + \lambda_2$$
$$0 \le \lambda_1 \perp x + \lambda_1 + \lambda_2 \ge 0$$
$$0 \le \lambda_2 \perp x + \lambda_1 + \lambda_2 \ge 0$$

where $x, \lambda_1, \lambda_2 \in \mathbb{R}$. As seen in Fig. 1 , the Lyapunov function jumps at $t = t^*$ for a solution $(x(t), \lambda^{\text{dec}}(t))$ and the Lyapunov function decreases ($V(t_+^*) > V(t_-^*)$). Then, consider $\lambda^{\text{inc}}(t)$ that jumps at $t = t^*$ where $\lambda_-^{\text{inc}} = \lambda_+^{\text{dec}}$ and $\lambda_+^{\text{inc}} = \lambda_-^{\text{dec}}$. The Lyapunov functions value increases after the jump at $t = t^*$ for the solution $(x(t), \lambda^{\text{inc}}(t))$ by construction as seen in Fig. 1.

If the function V jumps at a time t^* for one solution and its value decreases, then another solution exists, where V jumps at t^* and the function's value increases as illustrated in Example 8. Hence, the Lyapunov function cannot decrease monotonically along all solutions due to the multivalued nature of $\text{SOL}(Ex + c, F)$. For this reason, we focus on mappings W such that $W\text{SOL}(Ex + c, F)$ is single-valued. Using such mappings, one can parameterize Q, R, and r such that $Q\text{SOL}(Ex(t) + c, F)$, $\text{SOL}(Ex(t) + c, F)^T R\text{SOL}(Ex(t) + c, F)$, and $r^T\text{SOL}(Ex(t) + c, F)$ are single-valued for all t even when F is not a P-matrix.

Proposition 9: ([53], Proposition 3.9) Assume that $W\text{SOL}(q, F)$ is a singleton for all q where $W \in \mathbb{R}^{n_w\times m}$. Then, the map $q \mapsto W\text{SOL}(q, F)$ is a continuous piecewise linear function of q.

One can construct a Lyapunov function using a matrix W as in Proposition 9, where $Q\text{SOL}(Ex + c)$, $R\text{SOL}(Ex + c)$, and $r^T\text{SOL}(Ex + c)$ are singletons for all $x \in \mathbb{R}^n$ as follows:

$$V(x,\lambda) = x^T P x + 2x^T\tilde{Q}W\lambda + \lambda^T W^T\tilde{R}W\lambda + p^T x + \tilde{r}^T W\lambda + z \tag{12}$$

where $W \in \mathbb{R}^{n_w\times m}$, $\tilde{Q} \in \mathbb{R}^{n\times n_w}$, $\tilde{R} \in \mathbb{R}^{n_w\times n_w}$, $\tilde{r} \in \mathbb{R}^{n_w}$, and $W\text{SOL}(Ex + c, F)$ is a singleton. Next, it is shown that V is a nonsmooth, continuous piecewise quadratic function in x and is locally Lipschitz continuous, which are helpful properties in establishing stability results.

Lemma 10: The Lyapunov function[2] $V(x, \lambda(x))$ as in (12) is locally Lispchitz continuous in x. Furthermore, $\bar{V}(t) = V(x(t), \lambda(t)) \in AC([0, T])$ for all $T \ge 0$ for the solutions as in Definition 5.

Proof: Since $W\lambda(x)$ is Lipschitz continuous in x, $V(x, \lambda(x))$ is locally Lispchitz continuous in x. Because $x(t)$ is absolutely continuous and $V(x, \lambda(x))$ is locally Lipschitz continuous, V is absolutely continuous in time. ■

From this point onward, without loss of generality, the Lyapunov function as defined in (12) is used. Observe that if F is a P-matrix, one can trivially choose $W = I$. For many practical examples, it is possible to find such a matrix W. However, such a W is not guaranteed to exist when F is not a P-matrix. In Section V-C, it is shown how to generate W algorithmically.

Remark 11: Similar to the Lyapunov function, the input (7) is not necessarily continuous in time. If one desires a controller that is continuous in time, then the parametrization

$$u(\bar{x}, \lambda) = K\bar{x} + \tilde{L}W\lambda \tag{13}$$

leads to a controller u that is continuous in time. As discussed in Section VI-B, it is required that $D\text{SOL}(Ex + c, F)$ be a singleton for all x. Therefore, we restrict the controller to be of the form (13). For all of the examples in Section VI, the parametrization $L = \tilde{L}W$ is used.

[2] $\lambda(x)$ is the set-valued function $\lambda(x) = \text{SOL(Ex+c,F)}$.

B. Conditions for Stabilization

Now, conditions for stability in the sense of Lyapunov are constructed with the controller gains K and L as in (7), and the piecewise quadratic Lyapunov function V. These conditions will be the building blocks for the controller design method proposed in Section V.

Theorem 12: Consider the LCS (8), and the Lyapunov function (12) with W such that $W\text{SOL}(Ex+c,F)$ is a singleton for all x. Assume there exists a solution for every x_0 and $x_e=0$ is an equilibrium. If for all solutions $(x(t),\lambda(t))$,[3] there exist strictly positive constants γ_1,γ_2, matrices K,L[4] and a function V such that

$$\gamma_1||x(t)||_2^2 \le V(x(t),\lambda(t)) \le \gamma_2||x(t)||_2^2,$$

and $\frac{d\bar{V}(t)}{dt}\le 0$ for almost all t, then $x_e=0$ is Lyapunov stable. Furthermore, if there exists a strictly positive constant γ_3 such that $\frac{d\bar{V}(t)}{dt}\le -\gamma_3||x(t)||_2^2$ for almost all t, then $x_e=0$ is exponentially stable.

Proof: Let the solution $(x(t),\lambda(t))$ be arbitrary. Following Lemma 10, $\bar{V}(t)$ is absolutely continuous and almost everywhere differentiable on $[0,T]$ for all T. Then, we have

$$\bar{V}(t)=\bar{V}(0)+\int_0^t \dot{\bar{V}}(s)ds \le \bar{V}(0)$$

since $\dot{\bar{V}}\le 0$ for almost all $t\in\mathbb{R}^+$. Since V is bounded and nonincreasing, the rest follows from standard arguments for Lyapunov stability.

In order to prove exponential stability, observe that $\dot{\bar{V}}(t) \le -\gamma_3||x(t)||_2^2$. Hence, it follows that

$$||x(t)||_2^2 \le \frac{1}{\gamma_1}\bar{V}(0)-\frac{\gamma_3}{\gamma_1}\int_0^t ||x(s)||_2^2 ds.$$

Using Grönwall's inequality, it follows that

$$||x(t)||_2^2 \le \frac{1}{\gamma_1}\bar{V}(0)e^{-\frac{\gamma_3}{\gamma_1}t} \le \frac{\gamma_2}{\gamma_1}||x_0||_2^2 e^{-\frac{\gamma_3}{\gamma_1}t}.$$

Hence, we conclude that the equilibrium is exponentially stable. ■

Theorem 12 establishes sufficient conditions to stabilize the LCS in (8). In Section V, it is shown how Theorem 12 can be used to algorithmically synthesize a controller. Next, observe that an upper-bound always exists under certain assumptions.

Remark 13: If $c\ge 0$ and $z=0$, there exists a γ_2 such that $V(x,\lambda)\le\gamma_2||x||_2^2$, since $W\lambda(x)\le\rho||x||_2$ for all x for some ρ.

For this special case, an upper-bound always exists and one does not need to verify that V is upper-bounded when algorithmically synthesizing a controller (see Section V).

V. Controller Design as a BMI Feasibility Problem

Controller design for complementarity systems in the form of BMI's have been explored before for the case, where F in (8) is zero and without tactile feedback ($L=0$) [31]. In this section, these results are extended and it is shown how Theorem 12 can be used to algorithmically synthesize a controller when there is tactile feedback and the matrix F is nonzero. Then, the controller design problem is converted into a BMI feasibility problem. A convex optimization program is proposed to find a matrix W such that $W\text{SOL}(Ex+c,F)$ is a singleton for all x.

A. Sufficient Conditions for Stabilization

The sufficient conditions in Theorem 12 need to be satisfied for all solutions of the LCS (8). Now, we will transform them into matrix inequalities over two basic semialgebraic sets $\Gamma_{\text{SOL}}(E,F,c)$ and $\Gamma'_{\text{SOL}}(E,F,c)$. Define the set

$$\Gamma_{\text{SOL}}(E,F,c)=\{(\boldsymbol{x},\boldsymbol{\lambda}) : 0\le\boldsymbol{\lambda}\perp E\boldsymbol{x}+c+F\boldsymbol{\lambda}\ge 0\}$$

where $(\boldsymbol{x},\boldsymbol{\lambda})\in\Gamma_{\text{SOL}}(E,F,c)$ are represented as quadratic inequalities. Similarly, define the following set:

$$\begin{aligned}\Gamma'_{\text{SOL}}(E,F,c)=\{(\boldsymbol{x},\boldsymbol{\lambda},\dot{\boldsymbol{\lambda}})\big|\exists\boldsymbol{\rho},\boldsymbol{\mu}:\boldsymbol{\lambda}\in SOL(E\boldsymbol{x}+c,F)\\ E\dot{x}+F\dot{\boldsymbol{\lambda}}+\boldsymbol{\rho}=0,\ \boldsymbol{\lambda}_i\boldsymbol{\rho}_i=0,\dot{\boldsymbol{\lambda}}_i+\boldsymbol{\mu}_i=0\\ (E_i^T\boldsymbol{x}+F_i^T\boldsymbol{\lambda}+c_i)\boldsymbol{\mu}_i=0,\boldsymbol{\mu}_i\boldsymbol{\rho}_i=0\}\end{aligned} \tag{14}$$

where $\dot{x}=A\boldsymbol{x}+D\boldsymbol{\lambda}+a$ and $\boldsymbol{\mu},\boldsymbol{\rho}$ are slack variables. Here, $\dot{\boldsymbol{\lambda}}$ expresses the time derivative of the force. Next, we express the matrix inequalities over semialgebraic sets, where a method similar to construction of contact LCP's in ([24], Section 5.1.2.1) is used.

Proposition 14: If the inequalities

$$\gamma_1||\boldsymbol{x}||_2^2\le V(\boldsymbol{x},\boldsymbol{\lambda})\le\gamma_2||\boldsymbol{x}||_2^2,\ \forall(\boldsymbol{x},\boldsymbol{\lambda})\in\Gamma_{\text{SOL}} \tag{15}$$

$$\nabla_{\boldsymbol{x}}V(\boldsymbol{x},\boldsymbol{\lambda})^T\dot{x}+\nabla_{\boldsymbol{\lambda}}V(\boldsymbol{x},\boldsymbol{\lambda})^T\dot{\boldsymbol{\lambda}}\le 0,\ \forall(\boldsymbol{x},\boldsymbol{\lambda},\dot{\boldsymbol{\lambda}})\in\Gamma'_{\text{SOL}} \tag{16}$$

hold for the LCS (8), where $\dot{x}=A\boldsymbol{x}+D\boldsymbol{\lambda}+a$, then the following inequalities hold for all solutions $(x(t),\lambda(t))$ of the LCS

$$\gamma_1||x(t)||_2^2\le V(x(t),\lambda(t))\le\gamma_2||x(t)||_2^2 \tag{17}$$

$$\frac{d}{dt}V(x(t),\lambda(t))\le 0 \tag{18}$$

for almost all $t\ge 0$.

Proof: Consider an arbitrary solution, $(x(t),\lambda(t))$ of (8). First, we will show that (15) implies (17). From Definition 5, it follows that $\lambda(t)\in\text{SOL}(Ex+c,F)$ and $(x(t),\lambda(t))\in\Gamma_{\text{SOL}}(E,F,c)$ for almost all $t\ge 0$. The result follows from (15).

Next, we show that (16) implies (18). We show that

$$\lambda(t)\in\text{SOL}(Ex(t)+c,F) \tag{19}$$

$$\lambda_i(t)>0\Rightarrow E_i^T\dot{x}(t)+F_i^T\dot{\lambda}(t)=0 \tag{20}$$

$$E_i^Tx(t)+F_i^T\lambda(t)+c_i>0\Rightarrow\dot{\lambda}_i(t)=0 \tag{21}$$

$$\left.\begin{matrix}\lambda_i=0\\ E_i^Tx+F_i^T\lambda+c=0\end{matrix}\right\}\Rightarrow\begin{matrix}\dot{\lambda}_i=0\ \text{ or}\\ E_i^T\dot{x}+F_i^T\dot{\lambda}=0\end{matrix} \tag{22}$$

hold for almost all $t\ge 0$, where dependency on t in (22) is suppressed for space limitations, $\dot{\lambda}(t)=\frac{d\lambda}{dt}$, and (19) directly follows from the definition of solution.

[3] Dependence on x_0 and LCS parameters is suppressed.

[4] $\frac{d\bar{V}(t)}{dt}$ depends on K and L since $\dot{x}$ is a function of K and L.

We define $n_i(t) = E_i^T x(t) + F_i^T \lambda(t) + c$ for notational simplicity. To prove (20)–(22), observe that for almost all $t \geq 0$, there exists an $\epsilon > 0$ such that both $\lambda_i(t)$ and $n_i(t)$ are continuous in the interval $[t-\epsilon, t+\epsilon]$. For almost all $t \geq 0$ if $\lambda_i(t) > 0$, then $n_i(t) = 0$ for a neighborhood around t hence $E_i^T \dot{x}(t) + F_i^T \dot{\lambda}(t) = 0$ and (20) follows. Similarly observe that if $n_i(t) > 0$, then $\lambda(t) = 0$ and $\dot{\lambda}(t) = 0$ as in (21). Equation (22) follows from the the fact that both $\lambda_i(t)$ and $n_i(t)$ cannot be positive at the same time.

Suppose (19)–(22) hold at some time t^* and consider $x_* = x(t^*), \lambda_* = \lambda(t^*), \dot{\lambda}_* = \lambda(t^*)$ and $\dot{x}_* = \dot{x}(t^*)$. We will show that $(x_*, \lambda_*, \dot{\lambda}_*) \in \Gamma'_{\text{SOL}}(E, F, c)$.

There are three cases. First consider the case, where $\lambda_{i,*} > 0$ and therefore $(E_i^T x_* + F_i^T \lambda_* + c_i) = 0$. Observe that all equalities in (14) are satisfied with $\rho_{i,*} = 0$ and $\mu_{i,*} = -\dot{\lambda}_{i,*}$.

For the case, where $\lambda_{i,*} = 0$ and $(E_i^T x_* + F_i^T \lambda_* + c_i) > 0$, all equalities are satisfied with $\rho_{i,*} = -E_i^T \dot{x}_* - F\dot{\lambda}_{i,*}$ and $\mu_{i,*} = 0$.

For the last case, where both $(E_i^T x_* + F_i^T \lambda_* + c_i) = \lambda_{i,*} = 0$, the equalities are satisfied with either $\rho_{i,*} = 0$, $\mu_{i,*} = -\dot{\lambda}_{i,*}$ or $\rho_{i,*} = -E_i^T \dot{x}_* - F\dot{\lambda}_{i,*}$, $\mu_{i,*} = 0$.

Since the implications hold for almost all t, we conclude that $(x(t), \lambda(t), \dot{\lambda}(t)) \in \Gamma'_{\text{SOL}}$ for almost all $t \geq 0$. The result follows from (16). ■

Following Proposition 14 and Theorem 12, if the matrix inequalities (see Appendix A for the full derivation) over basic semialgebraic sets (15), (16) are satisfied, one can conclude that the equilibrium x_e is Lyapunov stable. Similarly, one can show that the equilibrium is exponentially stable if the left side of (16) is upper-bounded by $-\gamma_3 ||\boldsymbol{x}||_2^2$ as in Theorem 12.

B. Control Design

Now, the sets $\Gamma_{\text{SOL}}(E, F, c)$, $\Gamma'_{\text{SOL}}(E, F, c)$ are defined and it is assumed that there is access to a matrix W. The BMI feasibility problem with strictly positive constants γ_1, γ_2 and nonnegative γ_3 can be formulated as follows:

$$\text{find } V(\boldsymbol{x}, \boldsymbol{\lambda}), K, L \tag{23}$$

$$\text{s.t. } \gamma_1 ||\boldsymbol{x}||_2^2 \leq V(\boldsymbol{x}, \boldsymbol{\lambda}) \leq \gamma_2 ||\boldsymbol{x}||_2^2,\ (\boldsymbol{x}, \boldsymbol{\lambda}) \in \Gamma_{\text{SOL}}(E, F, c)$$

$$\frac{dV}{dt} \leq -\gamma_3 ||\boldsymbol{x}||_2^2,\ (\boldsymbol{x}, \boldsymbol{\lambda}, \dot{\boldsymbol{\lambda}}) \in \Gamma'_{\text{SOL}}(E, F, c)$$

with the function $V(\boldsymbol{x}, \boldsymbol{\lambda})$ as in (12) and

$$\frac{dV}{dt} = 2\boldsymbol{x}^T P(A\boldsymbol{x} + D\boldsymbol{\lambda} + a) + 2(A\boldsymbol{x} + D\boldsymbol{\lambda} + a)^T \tilde{Q} W \boldsymbol{\lambda} + 2\boldsymbol{x}^T \tilde{Q} W \dot{\lambda} + 2\boldsymbol{\lambda}^T W^T \tilde{R} W \dot{\boldsymbol{\lambda}} + p^T \dot{x} + \tilde{r} W_i^T \dot{\boldsymbol{\lambda}}$$

with the controller as in (13). Here, V encodes the nonsmoothness of the problem structure, mirroring the structure of the LCS, and allow tactile feedback design without exponential enumeration. This is an appealing middle ground between the common Lyapunov function of our prior work [8], and purely hybrid approaches [7], [58]. Whereas methods like our prior work are more conservative than the proposed method (Example 3.3., [53]), purely hybrid methods are less conservative at the cost of additional computation. Here, it is possible to assign a different Lyapunov function and a control policy for each mode while avoiding mode enumeration so the approach can scale to large number of contacts m unlike purely hybrid approaches.

Notice that the inequality with $\frac{dV}{dt}$ in (23) is a BMI because of the bilinear terms such as PA where A as in (8) depends on the gain matrix K as discussed in Section III. In (23), the problem of designing a control policy is formulated as finding a feasible solution for a set of BMIs. The sets $\Gamma_{\text{SOL}}(E, F, c)$ and $\Gamma'_{\text{SOL}}(E, F, c)$ are incorporated via the S-procedure.

C. Computing W via Polynomial Optimization

Until this point, it is assumed that there is access to a W such that $W\text{SOL}(Ex + c, F)$ is a singleton for all $x \in \mathbb{R}^n$. If F is a P-matrix, one can always pick $W = I$ since $\text{SOL}(Ex + c, F)$ is a singleton for any x as discussed earlier. For the non-P case, one can always trivially pick $W = 0$, which turns the Lyapunov function (12) into a common Lyapunov function, and controller (7) into a nonswitching state feedback controller. On the other hand, it is clearly better to search over a wider range of Lyapunov functions and controllers [57], [53]. Hence it is desired to maximize the rank of W. More precisely, consider the following optimization problem:

$$\max_W \quad \text{rank}(W)$$

$$\text{subject to} \quad W\text{SOL}(q, F) \text{ is a singleton for all } q.$$

To solve this problem, an algorithm based in a sequence of convex optimization problems is proposed. First, consider the following subproblem

$$\text{find}_w \quad \text{s.t.} \quad w^T \text{SOL}(q, F) \text{ is a singleton for all } q \tag{24}$$

where $w \in \mathbb{R}^m$. Using this subproblem, we will construct an algorithm to find matrices W. Notice that a w such that $|w^T(\lambda_{1,q} - \lambda_{2,q})| = 0$ holds for all q, and all $\lambda_{1,q}, \lambda_{2,q} \in \text{SOL}(q, F)$ satisfies (24). Next, we demonstrate that it is sufficient to satisfy $|w^T(\lambda_{1,q} - \lambda_{2,q})| \leq \eta$ for any $\eta > 0$ to satisfy (24).

Proposition 15: Suppose that for some w, the following inequalities hold for all q, all $\lambda_{1,q}, \lambda_{2,q} \in \text{SOL}(q, F)$:

$$\begin{aligned}(\eta + w^T(\lambda_{1,q} - \lambda_{2,q}))(\lambda_{1,q}^T \lambda_{1,q} + \lambda_{2,q}^T \lambda_{2,q}) \geq 0 \\ (\eta - w^T(\lambda_{1,q} - \lambda_{2,q}))(\lambda_{1,q}^T \lambda_{1,q} + \lambda_{2,q}^T \lambda_{2,q}) \geq 0\end{aligned} \tag{25}$$

where $\eta > 0$ is a constant slack parameter. Then, $w^T \text{SOL}(q, F)$ is a singleton for all q.

Proof: Observe that

$$\lambda \in \text{SOL}(q, F) \Rightarrow \alpha\lambda \in \text{SOL}(\alpha q, F)$$

for all $\alpha \geq 0$. We will show that the positive homogeneity property leads to

$$|w^T(\lambda_{1,q} - \lambda_{2,q})| \leq \eta\ \forall q \Rightarrow |w^T(\lambda_{1,q} - \lambda_{2,q})| = 0\ \forall q. \tag{26}$$

Assume that there exists $\eta^* > 0$ such that $|w^T(\lambda_{1,q^*} - \lambda_{2,q^*})| = \eta^*$ for some q^*. Pick $\alpha^* > 0$ such that $\alpha^* \eta^* > \eta$ and $|w^T(\alpha^* \lambda_{1,q^*} - \alpha^* \lambda_{2,q*})| = \alpha^* \eta^* > \eta$. Due to the positive homogeneity property, there exists $\lambda_{1,\alpha q^*}$ and $\lambda_{2,\alpha q^*}$ such that $|w^T(\lambda_{1,\alpha q^*} - \lambda_{2,\alpha q*})| = \alpha^* \eta^* > \eta$. This leads to a contradiction.

Algorithm 1: Find W.

Require: F

Initialization : $N \leftarrow I$, $W = [\,]$, $r = \mathbf{1}$, $w = \mathbf{1}$

while $\min r^T N^T w \neq 0$ **do**
  $r \sim U(0,1)$
  Solve (27) and obtain w
  if $\min r^T N^T w < 0$ **then**
    $W \leftarrow \begin{bmatrix} W \\ w^T \end{bmatrix}$
    Calculate N based on $\mathcal{N}(W)$
  end if
end while
return W

Next, we consider q such that $(\lambda_{1,q}^T \lambda_{1,q} + \lambda_{2,q}^T \lambda_{2,q}) > 0$. It follows from (25) that $|w^T(\lambda_{1,q} - \lambda_{2,q})| \leq \eta$ hence $|w^T(\lambda_{1,q} - \lambda_{2,q})| = 0$. If $(\lambda_{1,q}^T \lambda_{1,q} + \lambda_{2,q}^T \lambda_{2,q}) = 0$, then $\lambda_{1,q} = \lambda_{2,q} = 0$ and it trivially holds that $w^T \lambda_{1,q} = w^T \lambda_{2,q}$. Therefore, for any w such that (25) holds, $w^T \lambda_{1,q} = w^T \lambda_{2,q}$ also holds for all q. Hence, $w^T SOL(q, F)$ is a singleton for all q. ■

Finding a w such that (25) holds can be reduced to a polynomial optimization program [see Appendix B, (39)] and any vector w that satisfies (25) also satisfies (24). Experimentally, we found that use of the slack variable η was helpful to avoid numerical difficulties in the solvers. The solvers (Mosek [59], SeDuMi [60]) had trouble verifying the status of the problem (feasible or infeasible) when $\eta = 0$. The $(\lambda_{1,q}^T \lambda_{1,q} + \lambda_{2,q}^T \lambda_{2,q})$ terms in (25) are introduced because there are degree two S-procedure terms [as shown in (39)] and the inequalities must be at least degree two to use such S-procedure terms.

Given a matrix $W_d \in \mathbb{R}^{s \times m}$, one can utilize Proposition 15 in order to find a vector w such that $w^T \text{SOL}(q, F)$ is a singleton (for all q) and w^T is linearly independent with the rows of W_d. Consider the optimization problem:

$$\begin{aligned} \min_{w,\eta} \quad & r^T N^T w \qquad (27) \\ \text{subject to} \quad & (\eta + w^T(\boldsymbol{\lambda}_1 - \boldsymbol{\lambda}_2))(\boldsymbol{\lambda}_1^T \boldsymbol{\lambda}_1 + \boldsymbol{\lambda}_2^T \boldsymbol{\lambda}_2) \geq 0 \\ & (\eta - w^T(\boldsymbol{\lambda}_1 - \boldsymbol{\lambda}_2))(\boldsymbol{\lambda}_1^T \boldsymbol{\lambda}_1 + \boldsymbol{\lambda}_2^T \boldsymbol{\lambda}_2) \geq 0 \\ & \text{for } \boldsymbol{\lambda}_1, \boldsymbol{\lambda}_2 \in \text{SOL}(\boldsymbol{q}, F) \\ & |w_i| \leq 1, \ \forall i, \ \eta \geq 0 \end{aligned}$$

where r is a random vector with entries sampled from uniform distribution ($r_i \sim U(0,1)$), N is a basis for the nullspace of W_d ($\mathcal{N}(W_d)$), $\boldsymbol{\lambda}_1, \boldsymbol{\lambda}_2, \boldsymbol{q}$ are indeterminates, and the set inclusion is incorporated via the S-procedure for the first two inequalities [Appendix B, (40)]. Randomness is introduced in (27) in order to ensure that the objective function is almost surely strictly negative. More precisely, a linear objective that is strictly negative if any N such that $Nw \neq 0$ exists is needed and projection onto a random vector r ensures this with probability one.

Proposition 16: Consider W_d and the optimization (27). If there exists a w such that the constraints hold, and w^T is linearly independent with the rows of W_d, then $\min r^T N^T w < 0$ almost surely.

Proof: Assume there exists a w that is feasible for optimization problem (27) and w^T is linearly independent with the rows of W_d. Then, $||N^T w|| > 0$ and $r^T N^T w \neq 0$ with probability 1. By homogeneity, an optimal w_* can be found such that $r^T N^T w_* < 0$. ■

We now introduce Algorithm 1 based on Proposition 16. The algorithm almost surely finds a new linearly independent vector that satisfies the constraints in (27) if it exists and terminates when there are not any left. Notice that the randomization process affects the outcome (W) but we are only interested in finding a W such that $W\text{SOL}(q, F)$ is a singleton for all q hence this effect can be neglected.

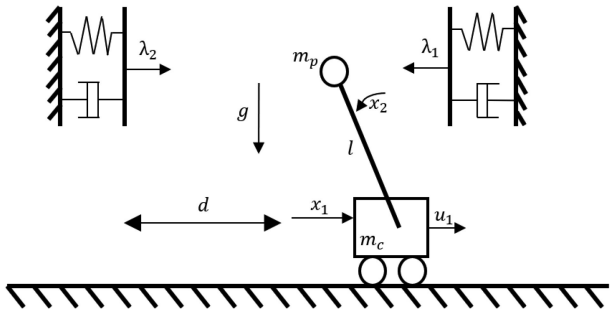

Fig. 2. Benchmark problem: Regulation of the cart-pole system to the origin with soft walls.

VI. Numerical Examples

In this article, the YALMIP [61] toolbox and PENBMI [62] are used to formulate and solve BMIs. SeDuMi [60] and Mosek [59] are used for solving the SDPs. PATH [63] has been used to solve the LCPs when performing simulations. MATLAB's stiff solver "ode15 s" is used while performing simulations of the LCS models and Euler's method with stepsize 10^{-4} is used for the nonlinear models. The code for all examples is available[5] and examples are provided with a video depiction.[6] The experiments are done on a desktop computer with the processor *Intel i7-9700* and *16 GB RAM*. We have reported the offline computation times for all of the examples and emphasize that our controller only requires only a few addition and multiplication operations when running online and is applicable in real time context after the offline computations are done.

A. Cart-Pole With Soft Walls

Consider the cart-pole system, where the goal is to balance the pole and regulate the cart to the center, where there are frictionless walls, modeled via spring contacts, on both sides. This problem, or a slight variation of it, has been used as a benchmark in control through contact [7], [64], [65] and the model is shown in Fig. 2.

First, the model where there is no damping is analyzed. In this model, the x_1 is the position of the cart, x_2 is the angle of the

[5][Online]. Available: https://github.com/AlpAydinoglu/cdesign

[6][Online]. Available: https://www.youtube.com/watch?v=CpYZcinYuQM

pole, and x_3, x_4 are their respective time derivatives. The input u_1 is a force applied to the cart, and the contact forces of the walls are represented with λ_1 and λ_2, leading to the LCS

$$\dot{x}_1 = x_3 \tag{28}$$

$$\dot{x}_2 = x_4 \tag{29}$$

$$\dot{x}_3 = \frac{gm_p}{m_c}x_2 + \frac{1}{m_c}u_1 \tag{30}$$

$$\dot{x}_4 = \frac{g(m_c+m_p)}{lm_c}x_2 + \frac{1}{lm_c}u_1 + \frac{1}{lm_p}\lambda_1 - \frac{1}{lm_p}\lambda_2 \tag{31}$$

$$0 \le \lambda_1 \perp lx_2 - x_1 + \frac{1}{k_1}\lambda_1 + d \ge 0$$

$$0 \le \lambda_2 \perp x_1 - lx_2 + \frac{1}{k_2}\lambda_2 + d \ge 0$$

where $k_1 = k_2 = 10$ are stiffness parameters of the soft walls, $g = 9.81$ is the gravitational acceleration, $m_p = 0.1$ is the mass of the pole, $m_c = 1$ is the mass of the cart, $l = 0.5$ is the length of the pole, and $d = 0.1$ represents where the walls are. Observe that the model has absolutely continuous solutions following Proposition 6. For this model, we solve the feasibility problem (23) and find a controller of the form $u(x,\lambda) = Kx + L\lambda$ that regulates the model to the origin with $K = \begin{bmatrix}3.69 & -46.7 & 3.39 & -5.71\end{bmatrix}$ and $L = \begin{bmatrix}-13.98 & 13.98\end{bmatrix}$. The algorithm succeeded in finding a feasible controller in 0.72 s. Additionally, we have tried to find a pure state feedback controller ($L = 0$) and, as formulated, failed to find such a controller for 1000 trials starting from different initial conditions. Due to the nonconvexity of the BMI, this does not guarantee that such a controller-Lyapunov function pair does not exist, but demonstrates that the optimization problem is harder to solve in more conservative settings.

As a comparison, consider an LQR controller with penalty on the state $Q = 100I$ and penalty on the input $R = 1$, which is given as $K_{\text{LQR}} = \begin{bmatrix}10 & -91.77 & 16.28 & -22.69\end{bmatrix}$. Both contact-aware and LQR controllers are tested on the nonlinear plant for 100 initial conditions, where $x_2(0) = 0$, and $x_1(0), x_3(0), x_4(0)$ are uniformly distributed $(10x_1(0), \frac{1}{4}x_3(0), x_4(0) \sim U[-1, 1])$. The LQR controller was successful only 31% of the time, whereas our contact-aware policy was successful 87% of the time. In Fig. 3, an example is presented where both LQR and contact-aware policy start from the same initial conditions and LQR fails, whereas our policy is successful. Our method is compared with LQR, which uses linearization and thus ignores potential contact events. Our controller is a contact-aware analogue to nonswitching state-feedback controllers such as LQR. In our comparison, the LQR controller acts as a stand-in for these methods, which do not explicitly consider the nonsmooth structure of the system.

Then, two different cases with higher stiffness values are explored. First, a controller is designed for the case where $k_1 = k_2 = 100$ with the controller gains

$$K_{100} = \begin{bmatrix}3.69 & -48.78 & 2.36 & -9.96\end{bmatrix}$$

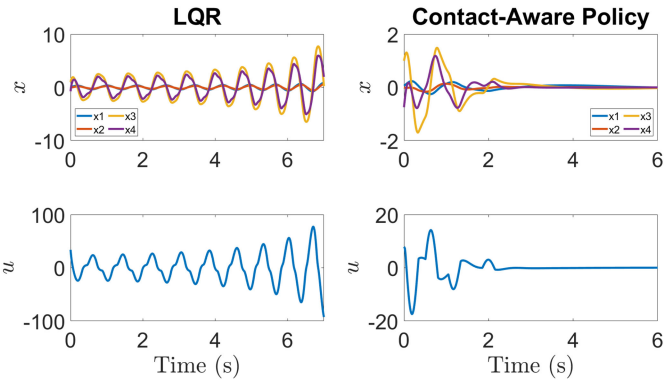

Fig. 3. Performance of LQR and contact-aware policy starting from the same initial condition for the cart-pole with soft walls example. LQR is unstable, whereas contact-aware policy is successful.

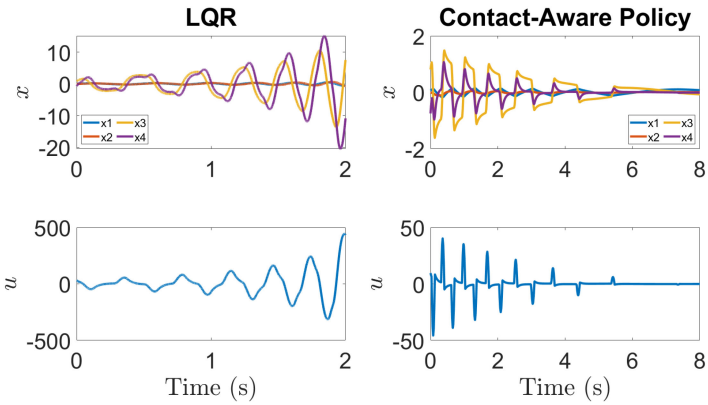

Fig. 4. Comparison of the LQR controller and contact-aware policy for $k_1 = k_2 = 100$. The LQR controller fails to stabilize the system whereas contact-aware policy is successful.

$$L_{100} = \begin{bmatrix}-14.14 & 14.14\end{bmatrix}.$$

The performance of the contact-aware controller is demonstrated against the previously designed LQR on the nonlinear plant in Fig. 4.

One more set of experiments is presented, where $k_1 = k_2 = 1000$ and a controller is designed with the gains

$$K_{1000} = \begin{bmatrix}0.45 & -40.23 & 0.86 & -25.50\end{bmatrix}$$

$$L_{1000} = \begin{bmatrix}-14.14 & 14.14\end{bmatrix}.$$

The performance of the contact-aware controller is demonstrated against the previously designed LQR on the nonlinear plant in Fig. 5. Notice that it is possible to design controllers for stiffer contacts, but stiff, near-impulsive contact events resolve very quickly and that measurement and rapid response may not be practical.

Next, inspired by [66], consider the case where damping term, b, is nonzero. The system dynamics are modeled as in (28)–(31) with the following complementarity constraints:

$$0 \le \lambda_1 \perp -kx_1 + klx_2 - bx_3 + blx_4 + kd + \lambda_1 + \gamma_1 \ge 0$$

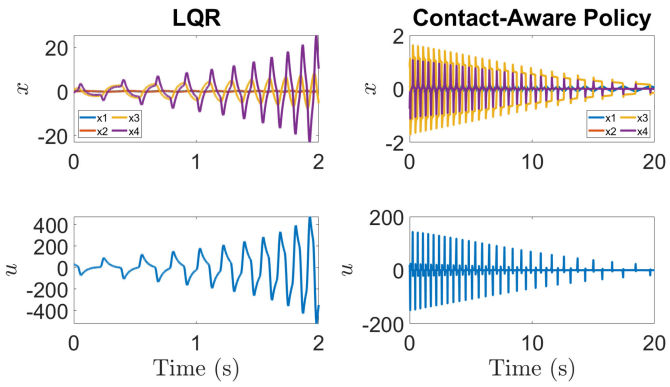

Fig. 5. Comparison of the LQR controller and contact-aware policy for $k_1 = k_2 = 1000$. The LQR controller fails to stabilize the system whereas contact-aware policy is successful.

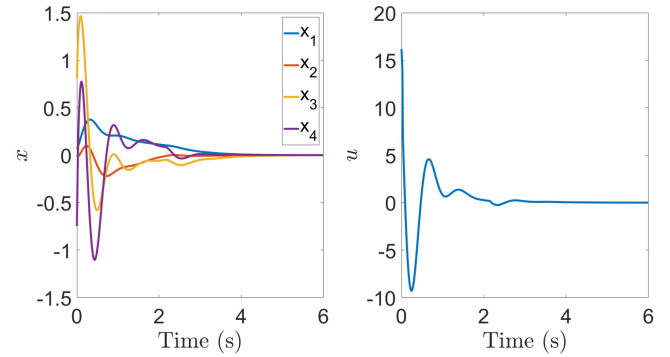

Fig. 6. Performance of tactile feedback controller with damping. Contact-aware policy successfully stabilizes the nonlinear plant.

$$0 \le \gamma_1 \perp Mx_1 - Mlx_2 - Md + \gamma_1 \ge 0$$
$$0 \le \lambda_2 \perp kx_1 - lkx_2 + bx_3 - blx_4 + kd + \lambda_2 + \gamma_2 \ge 0$$
$$0 \le \gamma_2 \perp -Mx_1 + Mlx_2 - Md + \gamma_2$$

where a large positive constant $M = 1000$ is introduced and the slack variables γ_1 and γ_2 to capture the affect of damper. As M increases the model approximates the spring-damper model [66] better. In this model, consider $b = 1$, $k = 10$, $m_p = m_c = 1$, $g = 9.81$, $l = 0.5$, $d = 0.1$. For this model, we solve the feasibility problem (23) and find a controller of the form $u(x, \lambda) = Kx + L\lambda$ that regulates the model to the origin with $K = \begin{bmatrix} 8.47 & -64.54 & 10.36 & -9.69 \end{bmatrix}$ and $L = \begin{bmatrix} -4.8 & 0 & 4.76 & 0 \end{bmatrix}$ in 384 s. The performance of the controller is demonstrated on the nonlinear plant in Fig. 6.

B. Partial State Feedback

Consider a model that consists of three carts on a frictionless surface as in Fig. 8. The cart on the left is attached to a pole and the cart in the middle makes contact via soft springs. In this model, a spring only becomes active if the distance between the outer block and the block in the middle is less than some threshold. Here, x_1, x_2, x_3 represent the positions of the carts and x_4 is the angle of the pole. The corresponding LCS is

$$\ddot{x}_1 = \frac{gm_p}{m_1}x_4 + \frac{1}{m_1}u_1 - \frac{1}{m_1}\lambda_1$$
$$\ddot{x}_2 = \frac{\lambda_1}{m_2} - \frac{\lambda_2}{m_2}$$
$$\ddot{x}_3 = \frac{\lambda_2}{m_3} + \frac{u_2}{m_3}$$
$$\ddot{x}_4 = \frac{g(m_1 + m_p)}{m_1\, l}x_4 + \frac{u_1}{m_1\, l} - \frac{1}{m_1\, l}\lambda_1$$
$$0 \le \lambda_1 \perp x_2 - x_1 + \frac{1}{k_1}\lambda_1 \ge 0$$
$$0 \le \lambda_2 \perp x_3 - x_2 + \frac{1}{k_2}\lambda_2 \ge 0$$

where the masses of the carts are $m_1 = m_2 = m_3 = 1, g = 9.81$ is the gravitational acceleration, $m_p = 1.5$ is the mass of the pole, $l = 0.5$ is the length of the pole, and $k_1 = k_2 = 20$ are stiffness parameters of the springs. Observe that we have control over the outer blocks, but do not have any control over the block in the middle. Additionally, it is assumed that the middle block is not observed, and one can only observe the outer blocks and the contact forces. Notice that the model has absolutely continuous solutions following Proposition 6.

For this example, the feasibility problem (23) takes 9.3 s to solve with a controller of the form $u(x, \lambda) = Kx + L\lambda$ where

$$K = \begin{bmatrix} -2.8 & 0 & 6.6 & -263.1 & 6.4 & 0 & -2.1 & -30.2 \\ 11.5 & 0 & -12.1 & 12.1 & 2.6 & 0 & -4.7 & 6.6 \end{bmatrix}$$

$$L = \begin{bmatrix} -3.7 & -0.6 \\ -0.6 & 7.2 \end{bmatrix}.$$

Notice that we enforce sparsity on the controller K and do not use any feedback from the state x_2 or its derivative $\dot{x}_2$. This example demonstrates that tactile feedback can be used in scenarios, where full state information is lacking and also impact events can be used in order to stabilize the system. In Fig. 7, the performance of the controller is demonstrated.

C. Acrobot With Soft Joint Limits

As a third example, consider the classical underactuated acrobot, a double pendulum with a single actuator at the elbow (see [67] for the details of the acrobot dynamics). Additionally, soft joint limits are added to the model. Hence, we consider the model in Fig. 9

$$\dot{x} = Ax + Bu + D\lambda$$

where $x = (\theta_1, \theta_2, \dot{\theta}_1, \dot{\theta}_2)$, $\lambda = (\lambda_1, \lambda_2)$, and $D = \begin{bmatrix} 0_{2\times 2} \\ M^{-1}J^T \end{bmatrix}$ with $J^T = \begin{bmatrix} -1 & 1 \\ 0 & 0 \end{bmatrix}$. For this model, the masses of the rods are $m_1 = 0.5$, $m_2 = 1$, the lengths of the rods are $l_1 = 0.5$, $l_2 = 1$, and the gravitational acceleration is $g = 9.81$. The soft joint limits are modeled using the following complementarity

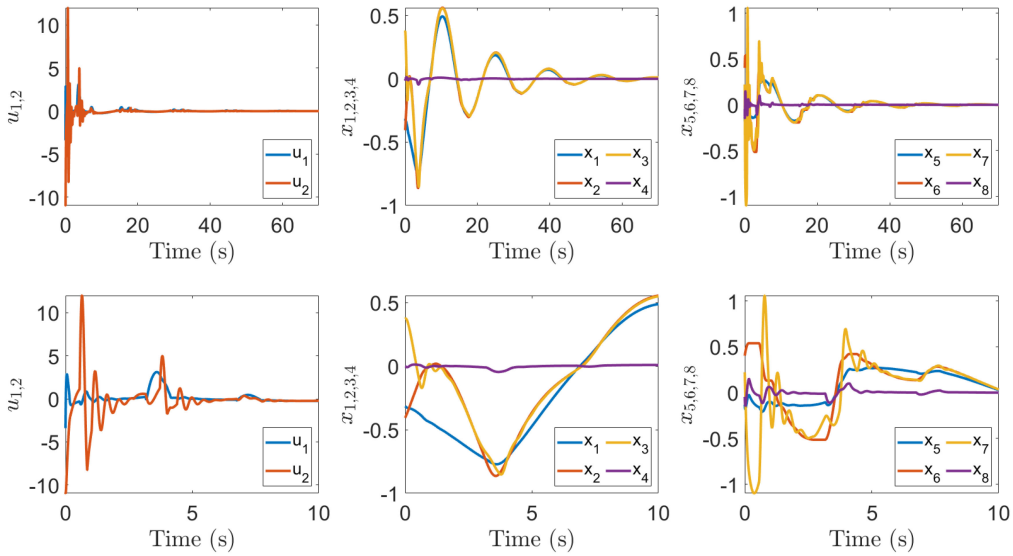

Fig. 7. Simulation with contact-aware policy for partial state-feedback example. The plots on the top row show the input and the state variables $(u(t), x(t))$ for the time interval $t = [0\ 60]$. Second row demonstrates the time interval $t = [0\ 10]$ for the same initial condition.

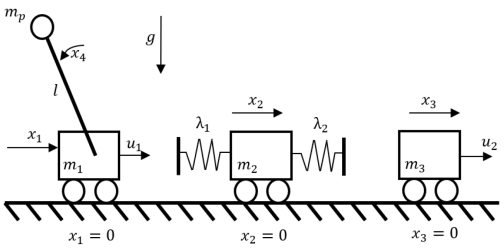

Fig. 8. Regulation of carts to their respective origins without observation of the middle cart.

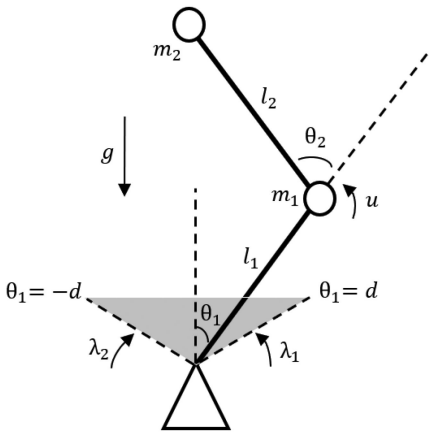

Fig. 9. Acrobot with soft joint limits.

constraints:

$$0 \leq d - \theta_1 + \frac{1}{k}\lambda_1 \perp \lambda_1 \geq 0$$

$$0 \leq \theta_1 + d + \frac{1}{k}\lambda_2 \perp \lambda_2 \geq 0$$

where $k = 1$ is the stiffness parameter and $d = 0.2$ is the angle that represents the joint limits in terms of the angle θ_1. Observe

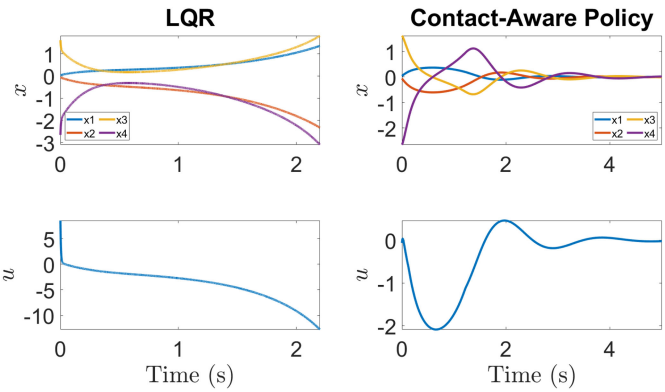

Fig. 10. Simulation of LQR and contact-aware policy starting from the same initial condition for the acrobot with soft joint limits example. LQR is unstable, whereas contact-aware policy is successful.

that the model has absolutely continuous solutions, $x(t)$, following Proposition 6 since F is a P-matrix.

For this example, we solve the feasibility problem (23) and obtain a controller of the form $u(x, \lambda) = Kx + L\lambda$ in 1.18 s with $K = \begin{bmatrix} 73.07 & 38.11 & 30.41 & 18.95 \end{bmatrix}$ and $L = \begin{bmatrix} -4.13 & 4.13 \end{bmatrix}$. For comparison, we also designed an LQR controller for the linear system, where the penalty on the state is $Q = 100I$ and the penalty on the input is $R = 1$ which is given as $K_{\text{LQR}} = \begin{bmatrix} 1476.3 & 851.68 & 548.81 & 334.43 \end{bmatrix}$. 100 trials were made on the nonlinear plant where initial conditions were sampled according to $x_1(0) = x_2(0) = 0$ and $x_3(0), x_4(0) \sim U[-0.05, 0.05]$. Out of these 100 trials, LQR was successful only 49% of the time, whereas our design was successful 87% of the time. In Fig. 10, a case where LQR fails and contact-aware policy is successful is presented.

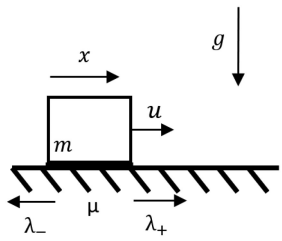

Fig. 11. Regulation task of a box standing on a surface with Coulomb friction.

D. Box With Friction

Consider a quasi-static model of a box on a surface, as in Fig. 11, where μ is the coefficient of friction between the box and the ground. Newtons's second law is approximated with a force balance equation with Coulomb friction and damping. The goal is to regulate the box to the center. This simple model serves as an example where F is not a P-matrix and the complementarity constraints have a dependency on the input u ($H \neq 0$). Here, x is the position of the box, u is the input, λ_+ is the positive component of the friction force, λ_- is the negative component of the friction force and γ is the slack variable

$$\begin{aligned}
\alpha\dot{x} &= u + \lambda_+ - \lambda_- \\
0 &\leq \gamma \perp \mu mg - \lambda_+ - \lambda_- \geq 0 \\
0 &\leq \lambda_+ \perp \gamma + u + \lambda_+ - \lambda_- \geq 0 \\
0 &\leq \lambda_- \perp \gamma - u - \lambda_+ + \lambda_- \geq 0
\end{aligned}$$

where $m = 1$ is the mass of the box, $g = 9.81$ is the gravitational acceleration $\mu = 0.1$ is the friction coefficient, and $\alpha = 4$ is the damping coefficient. Input delay is modeled with the low-pass filter

$$\begin{aligned}
\alpha\dot{x} &= \tau + \lambda_+ - \lambda_- \\
\dot{\tau} &= \kappa(u - \tau) \\
0 &\leq \gamma \perp \mu mg - \lambda_+ - \lambda_- \geq 0 \\
0 &\leq \lambda_t^+ \perp \gamma + \tau + \lambda_+ - \lambda_- \geq 0 \\
0 &\leq \lambda_t^- \perp \gamma - \tau - \lambda_+ + \lambda_- \geq 0
\end{aligned}$$

where $\kappa = 100$. Since F is not a P-matrix, we use Algorithm 1 and find $W = [0\ 1\ -1]$ such that $W\text{SOL}(q, F)$ is a singleton for all q in 8.09 s. For this example, W shows that the net friction force, $\lambda_+ - \lambda_-$ is always unique. Notice that the x-trajectory, $x(t)$ is unique, but the λ-trajectory, $\lambda(t)$ is not. Note that the closed-loop system has absolutely continuous solutions following Proposition 6 since it is enforced that $L\text{SOL}(Ex + c, F)$ is a singleton.

We can solve the feasibility problem in (23) in 22 s and find a controller of the form $u(x, \lambda) = Kx + L\lambda$ such that the system is Lyapunov stable with $K = \begin{bmatrix} -10.58 \end{bmatrix}$ and $L = \begin{bmatrix} 0 & 0.7 & -0.7 \end{bmatrix}$. In Fig. 12, the performance of the controller is demonstrated.

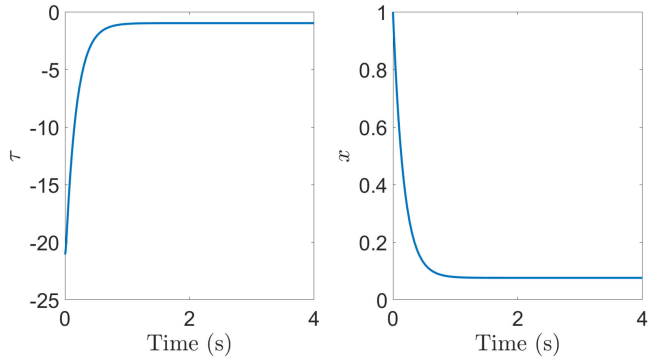

Fig. 12. Simulation of box with friction example. The equilibrium is Lyapunov stable and the state trajectory, $x(t)$ does not reach origin because of stiction.

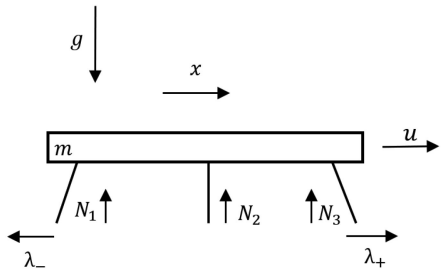

Fig. 13. Regulation task of a three legged table.

E. Three Legged Table

We examine a variation of Example D and consider a three legged table on a surface with Coulomb friction as in Fig. 13. In this model, the coefficient of friction values (μ_1, μ_2, μ_3) are different for each leg of the table. The normal forces at the legs of the table are denoted by (N_1, N_2, N_3) and sum of the normal forces are equal to the mass times gravitational acceleration, mg. The net friction force is unique in static situations but it is nonunique during sliding since individual normal forces, N_i, are nonunique. The task is regulating the three legged table to the center. Newton's second law is approximated with a force balance equation with Coulomb friction and damping as in the previous example. In this model, x is the position of the box, τ is the output of the low-pass filter, λ_+ is the positive component of the friction force, λ_- is the negative component of the friction force, γ is the slack variable, u is the force applied to the table

$$\alpha\dot{x} = \tau + \lambda_+ - \lambda_- \tag{32}$$

$$\dot{\tau} = \kappa(u - \tau) \tag{33}$$

$$0 \leq \gamma \perp \mu_1 N_1 + \mu_2 N_2 + \mu_3 N_3 - \lambda_+ - \lambda_- \geq 0 \tag{34}$$

$$0 \leq \lambda_+ \perp \gamma + \tau + \lambda_+ - \lambda_- \geq 0 \tag{35}$$

$$0 \leq \lambda_- \perp \gamma - \tau - \lambda_+ + \lambda_- \geq 0 \tag{36}$$

$$N_1 + N_2 + N_3 = mg \tag{37}$$

$$N_1, N_2, N_3 \geq 0 \tag{38}$$

where $(\mu_1, \mu_2, \mu_3) = (0.1, 0.5, 1)$ are the coefficient of friction parameters for the legs of the table, $m = 1$ is the mass of the box,

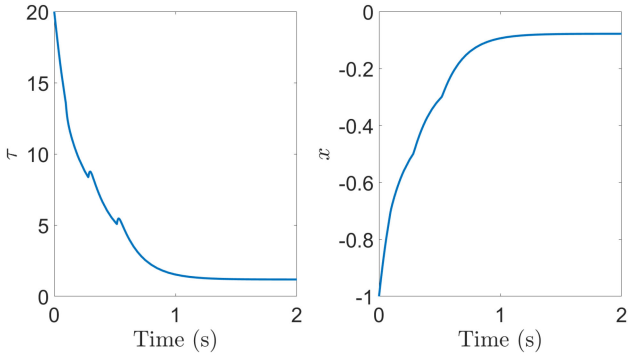

Fig. 14. Simulation of three legged table example for the normal forces $N(t) = [4.0910, 4.1195, 1.5995]$ for $t \in [0, 0.2992)$, $N(t) = [5.4033, 3.1206, 1.2861]$ for $t \in [0.2992, 0.5455)$ and $N(t) = [9.4866, 0.1770, 0.1464]$ for $t \in [0.5455, \infty)$.

$g = 9.81$ is the gravitational acceleration, $\alpha = 4$ is the damping coefficient, and $\kappa = 100$ is the filter coefficient. The constraints (37) and (38) are exchanged with

$$0 \leq N_1 \perp -mg + N_1 + N_2 + N_3 \geq 0$$
$$0 \leq N_2 \perp -mg + N_1 + N_2 + N_3 \geq 0$$
$$0 \leq N_3 \perp -mg + N_1 + N_2 + N_3 \geq 0$$

to be consistent with the framework. Note that extending the framework to LCS models with additional equality and inequality constraints as in (32)–(38) is straightforward but it is omitted for brevity.

After using Algorithm 1, we find that $W = [0\ 0\ 0\ 1\ 1\ 1]$ in 242.8 min. Observe that one can solve a smaller sized polynomial optimization that only includes N_1, N_2, N_3 in 3.08 s as the variables are decoupled from $\gamma, \lambda_+, \lambda_-$ and reach the same result. W shows that $N_1 + N_2 + N_3$ is unique, as expected since $N_1 + N_2 + N_3 = mg$. Note that $W\lambda = mg$ is a constant and the Lyapunov function (12) reduces to a common Lyapunov function. Based on the structure of W, unlike the previous example, the net force $\lambda_+ - \lambda_-$ is not unique, which is also expected due to the nonunique nature of normal forces. Notice that both the x-trajectory, $x(t)$ and λ-trajectory, $\lambda(t)$ are nonunique. The model has absolutely continuous solutions, $x(t)$ and $\tau(t)$, for fixed N_1, N_2, N_3 following Proposition 6. For this example, we only consider the case, where $N_1(t), N_2(t), N_3(t)$ are bounded piecewise constant functions with finitely many pieces hence $x(t)$ and $\tau(t)$ are absolutely continuous.

The feasibility problem (23) is solved in 19 s and a controller of the form $u(x, \lambda) = Kx + L\lambda$ is found such that the origin is Lyapunov stable with $K = \begin{bmatrix} -20.75 \end{bmatrix}$ and $L = \begin{bmatrix} 0 & 0.36 & -0.36 & 0 & 0 & 0 \end{bmatrix}$. The trajectories of the closed loop system are always absolutely continuous, since we enforce that $LSOL(Ex + c, F)$ is a singleton for fixed, arbitrary N_1, N_2, and N_3. In Fig. 14, observe that the force applied to the system (τ) is continuous even though u is not, due to the low-pass filter. The origin is Lyapunov stable and the trajectory does not reach origin because of stiction.

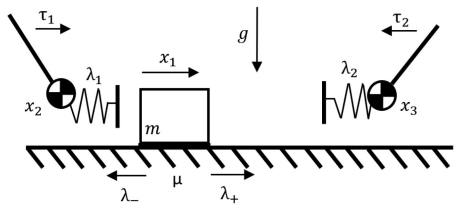

Fig. 15. 2-D manipulation task, where the goal is to regulate the position of the box on a surface with friction.

F. 2-D Simple Manipulation

Consider a quasi-static model of a box on a surface with friction parameter μ and two robotic arms that can interact with the box as in Fig. 15. Similar to the previous example, the force balance equation is used with Coulomb friction and damping to model the dynamics of the box. The velocity of the manipulators can be controlled directly with delayed inputs τ_1 and τ_2. In this model, x_1, x_2, x_3 represent the positions of the box, the left manipulator and the right manipulator, respectively. The contact forces λ_1 and λ_2 are nonzero if and only if the distance between the manipulators and the box is less than some threshold. The friction force consists of a positive component λ_+ and a negative component λ_-. We assume that we can not observe anything related to the box except the contact force between the manipulators and the box. The task is to regulate the box to the origin using the model

$$\alpha \dot{x}_1 = \lambda_1 - \lambda_2 + \lambda_+ - \lambda_-$$
$$\dot{x}_2 = \tau_1$$
$$\dot{x}_3 = \tau_2$$
$$\dot{\tau}_1 = \kappa(u_1 - \tau_1)$$
$$\dot{\tau}_2 = \kappa(u_2 - \tau_2)$$
$$0 \leq \lambda_1 \perp x_1 - x_2 + \frac{1}{k}\lambda_1 \geq 0$$
$$0 \leq \lambda_2 \perp x_3 - x_1 + \frac{1}{k}\lambda_2 \geq 0$$
$$0 \leq \gamma \perp \mu mg - \lambda_+ - \lambda_- \geq 0$$
$$0 \leq \lambda_+ \perp \gamma + \lambda_1 - \lambda_2 + \lambda_+ - \lambda_- \geq 0$$
$$0 \leq \lambda_- \perp \gamma - \lambda_1 + \lambda_2 - \lambda_+ + \lambda_- \geq 0$$

where $\kappa = 100, \mu = 0.1, m = 1, g = 9.81, \alpha = 1$, and $k = 100$. Since, F is not a P-matrix, we can construct the W matrix using the result in Example VI-D and obtain

$$W = \begin{bmatrix} 1 & 0 & 0 & 0 & 0 \\ 0 & 1 & 0 & 0 & 0 \\ 0 & 0 & 0 & 1 & -1 \end{bmatrix}.$$

Observing W, the net friction force, $\lambda_+ - \lambda_-$, is unique. The contact forces between the manipulators and the box, λ_1, λ_2 are also unique. Note that the closed-loop system has absolutely continuous solutions following Proposition 6, since it is enforced that $LSOL(Ex + c, F)$ is a singleton.

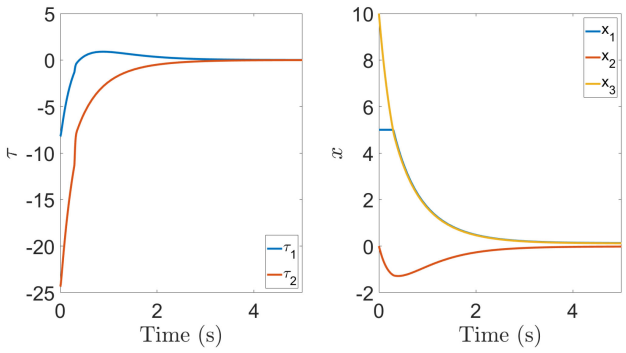

Fig. 16. Simulation results for 2-D simple manipulation example. The forces applied to the box (τ) are smooth even though u is not, due to the low-pass filter model.

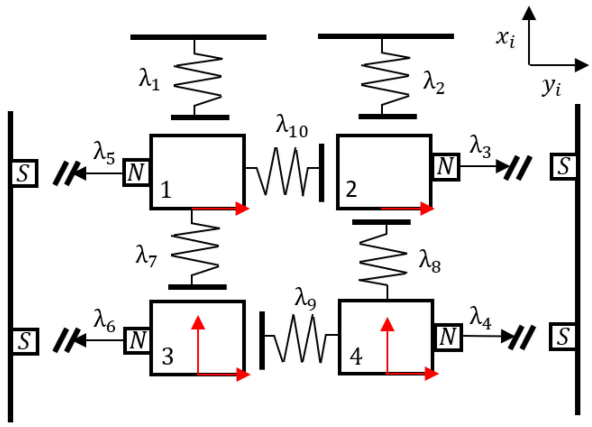

Fig. 17. Four carts example. The inputs that are applied to carts are represented by the red arrows.

Then, we solve the optimization problem to find a controller that asymptotically stabilizes the system to a small ball around the origin $\mathcal{B} = \{x : x^T x \leq 0.1\}$. The optimization problem finds a result in 7.06 minutes and a controller of the form $u(x, \lambda) = Kx + L\lambda$ that stabilizes the system is obtained with

$$K = \begin{bmatrix} 0 & -2.33 & -0.82 \\ 0 & -0.89 & -2.44 \end{bmatrix},$$

$$L = \begin{bmatrix} -0.26 & 0.06 & 0 & 0 & 0 \\ -0.06 & 0.27 & 0 & 0 & 0 \end{bmatrix}.$$

This example shows that the contact-aware policy can be used for systems with nonunique contact forces, e.g., quasi-static friction, where we do not have full state information. In Fig. 16, we demonstrate the performance of the controller.

G. Four Carts

As our last example, consider the system in Fig. 17. Here, (x_i, y_i) gives the position of the cart i. We approximate Newton's second law with a force balance equation for each cart. The contact forces $\lambda_1, \lambda_2, \lambda_7, \lambda_8, \lambda_9$, and λ_{10} are soft contacts that are represented by the springs and are nonzero if the objects are closer than a threshold. The forces $\lambda_3, \lambda_4, \lambda_5$, and λ_6 approximate attractive magnetic forces between the carts and the walls and similarly are nonzero if the distance between the carts and the walls is less than a threshold. The red arrows represent the input forces that can be applied to carts. We model this system with $n = 8$ states, and $m = 10$ contacts, where our goal is to show the performance of the proposed method on a high dimensional underactuated example that is unstable without any control action. The model parameters are $A = 0_{8\times 8}$, $c = 0_{10\times 1}$, $F = I_{10\times 10}$,

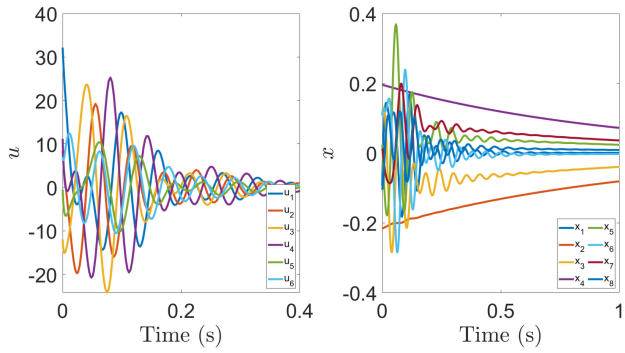

Fig. 18. Simulation of four carts example. The state trajectory, $x(t)$, asymptotically converges to the origin.

$$B = \begin{bmatrix} \begin{pmatrix} 1 & 0 \\ 0 & 0 \\ 0 & 1 \\ 0 & 0 \end{pmatrix} & 0_{4\times 3} \\ 0_{3\times 4} & I_{3\times 3} \end{bmatrix}$$

$$D = \begin{bmatrix} 0 & 0 & 0 & 0 & -1 & 0 & 0 & 0 & 0 & -1 \\ -1 & 0 & 0 & 0 & 0 & 0 & 1 & 0 & 0 & 0 \\ 0 & 0 & 1 & 0 & 0 & 0 & 0 & 0 & 0 & 1 \\ 0 & -1 & 0 & 0 & 0 & 0 & 0 & 1 & 0 & 0 \\ 0 & 0 & 0 & 0 & 0 & -1 & 0 & 0 & -1 & 0 \\ 0 & 0 & 0 & 0 & 0 & 0 & -1 & 0 & 0 & 0 \\ 0 & 0 & 0 & 1 & 0 & 0 & 0 & 0 & 1 & 0 \\ 0 & 0 & 0 & 0 & 0 & 0 & 0 & -1 & 0 & 0 \end{bmatrix},$$

$$E = \begin{bmatrix} 0 & -1 & 0 & 0 & 0 & 0 & 0 & 0 \\ 0 & 0 & 0 & -1 & 0 & 0 & 0 & 0 \\ 0 & 0 & -1 & 0 & 0 & 0 & 0 & 0 \\ 0 & 0 & 0 & 0 & 0 & 0 & -1 & 0 \\ 1 & 0 & 0 & 0 & 0 & 0 & 0 & 0 \\ 0 & 0 & 0 & 0 & 1 & 0 & 0 & 0 \\ 0 & 1 & 0 & 0 & 0 & -1 & 0 & 0 \\ 0 & 0 & 0 & 1 & 0 & 0 & 0 & -1 \\ 0 & 0 & 0 & 0 & -1 & 0 & 1 & 0 \\ -1 & 0 & 1 & 0 & 0 & 0 & 0 & 0 \end{bmatrix}.$$

Observe that the model has absolutely continuous solutions following Proposition 6. A controller of the form $u(x, \lambda) = Kx + L\lambda$ that stabilizes the system can be found. For this

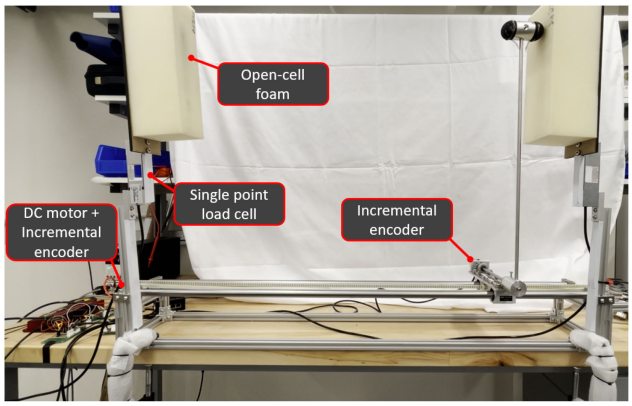

Fig. 19. Experimental setup for cart-pole with soft walls.

example, and higher dimensional examples in general, the initialization of the K and L matrices have a significant affect on the success of the algorithm. We initialized elements of K with sampling from uniform distribution ($K_{ij} \sim U[-100, 0]$). For one successful case, the algorithm terminates in 6 min and 58 s, but we also needed to run the algorithm approximately 20 h with random seeds to obtain a successful result. In Fig. 18, we present the performance of the controller.

VII. Experimental Validation

We demonstrate our contact-aware feedback controller on an experimental cart-pole system with soft walls shown in Fig. 19, replicating the system from Section VI-A. To generate linear motion of the cart, a dc motor is used with a belt drive. Linear motion of the cart was driven by torque-controlled dc motor and incremental encoders measured the positions of the cart and pole. We added soft walls and tactile sensing capabilities; open-cell polyurethane foam was used for the walls, and a "*Flintec PC42 Single Point Load Cell*" was used to measure the force exerted on the walls by the pole. Alternatively, sensors could have been placed on the pole itself.

A. System Model

We take the gravitational acceleration as $g = 9.81$, mass of the pole as $m_p = 0.35$, mass of the cart as $m_c = 0.978$, length of the center of mass location as $l_{\text{CoM}} = 0.4267$, the distance to the walls as $d = 0.35$ and and length of the pole as $l_p = 0.6$. After experimental trials, we identified the spring constant $k = 700$ and neglect the damping term ($b = 0$). The parameters of the LCS model are

$$A = \begin{bmatrix} 0 & 0 & 1 & 0 \\ 0 & 0 & 0 & 1 \\ 0 & 3.51 & 0 & 0 \\ 0 & 22.2 & 0 & 0 \end{bmatrix}, \; B = \begin{bmatrix} 0 \\ 0 \\ 1.02 \\ 1.7, \end{bmatrix}$$

$$D = \begin{bmatrix} 0 & 0 \\ 0 & 0 \\ 0 & 0 \\ 4.7619 & -4.7619 \end{bmatrix}, \; E = \begin{bmatrix} -1 & 0.6 & 0 & 0 \\ 1 & -0.6 & 0 & 0, \end{bmatrix}$$

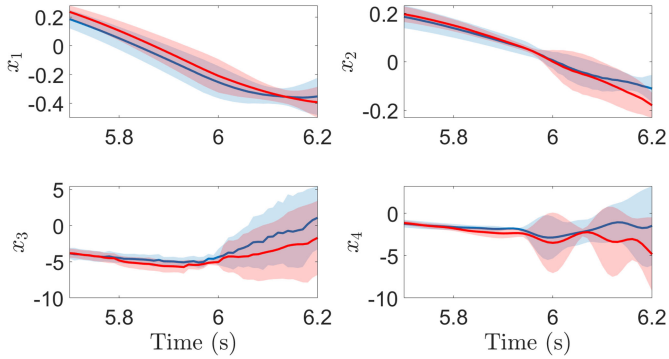

Fig. 20. Experiment 1—Trajectories around the impact event for all six trials. Blue represents contact-aware policy, red represents LQR, solid lines represent the respective means and shaded regions represent standard deviation. State distribution before the impact events are similar (≈ 2 cm difference in cart position and ≈ 1 degree difference in pole angle). The velocity of the cart (x_3) is significantly higher for contact-aware policy after the impact.

$$F = \begin{bmatrix} 0.0014 & 0 \\ 0 & 0.0014 \end{bmatrix}, \; c = \begin{bmatrix} 0.35 \\ 0.35 \end{bmatrix}.$$

B. Experiments

Three sets of experiments are performed. For the first two, our method is compared against an LQR controller where $K_{\text{LQR}} = \begin{bmatrix} 3.16 & -40.78 & 4.3 & -7.67 \end{bmatrix}$. The contact-aware policy is designed such that $K = K_{\text{LQR}}$ is enforced and a contact gain matrix $L = \begin{bmatrix} -10.02 & 10.02 \end{bmatrix}$ is found. It may be impossible to find a contact gain L with a fixed K in general, but $K = K_{\text{LQR}}$ was enforced for a more fair comparison with LQR. If we let the BMI design search for both K and L, we can potentially get a better solution, though BMI enforces stability versus optimality. Then, we perform between 6 and 10 trial experiments depending on the setup, after which we observed deterioration of the experimental setup due to the violence of the impact events that occurred when the LQR controller failed to stabilize the system. While performing these experiments, sensor readings below 1 N are considered as 0 N to neglect the effect of oscillations that occur after the impact events. For the third experiment, we repeat Experiment 1 without thresholds on the sensor readings.

Experiment 1. We execute balancing controllers, which attempt to stabilize the system to the origin and evaluate their performance by introducing large perturbations that lead to contact events. First, the system is started in the upright position at the right wall, $x_0^T = \begin{bmatrix} 0.35 & 0 & 0 & 0 \end{bmatrix}$. Then, a control input[7] is applied such that the pole impacts the left wall with high speed and close to upright position.

We repeated this experiment 6 times for both policies. In Fig. 20, we demonstrate that the initial conditions for all trials (at $t = 5.7$) are similar. The mean difference is 0.05, 0.01, 0.01, 0.04, respectively, for x_1, x_2, x_3, x_4. The LQR policy failed

[7]We apply the control input $u = K(x - x_s)$, where $x_s^T = \begin{bmatrix} 0 & 0.35 & 0 & 0 \end{bmatrix}$; hence, the cart moves towards the left wall; then, we switch back to $x_s^T = \begin{bmatrix} 0 & 0 & 0 & 0 \end{bmatrix}$.

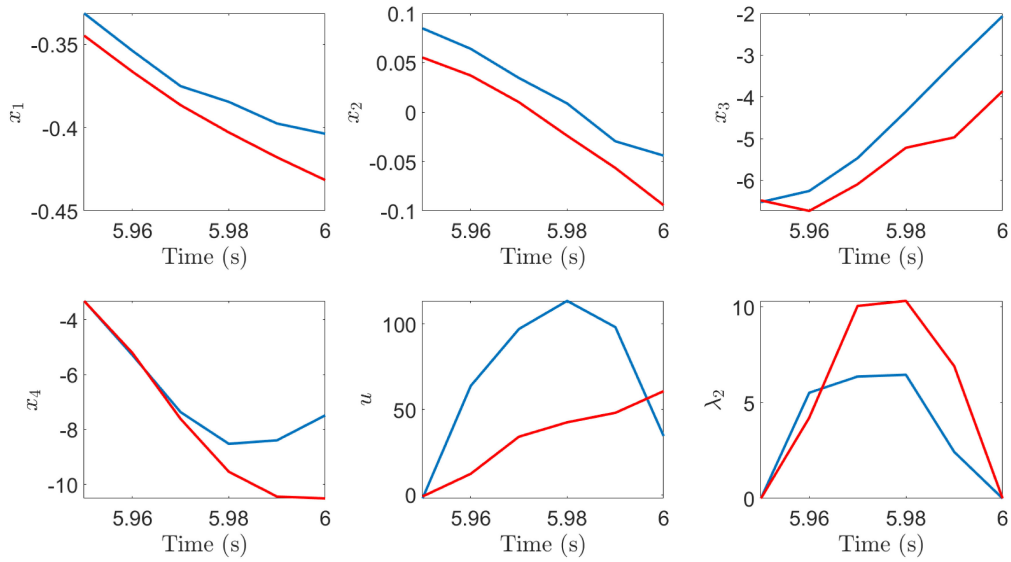

Fig. 21. Experiment 1—Blue represents the contact-aware policy and red represents LQR. Contact-aware policy (u) starts pushing the cart in the positive direction aggressively as soon as impact starts (λ_2) in order to catch the falling pole causing a big increase in the cart velocity (x_3). As a result of contact-aware policy, the angular speed of pole is closer to zero (x_4). The contact-aware policy also mitigates the impact (λ_2).

in all $(0/6)$ of the trials, whereas contact-aware policy was always successful $(6/6)$. Since the policies are identical when not in contact, we focus our analysis and plots on the brief time windows ($t = [5.7, 6.2]$ as in Fig. 20), which contain impact events. The contact-aware policy results in a significant increase in cart velocity (during the impact event) in order to catch the falling pole (the mean cart velocity for contact-aware policy is 2.76 m/s higher than LQR at $t = 6.2$). Similarly, the mean angular velocity of the pole with LQR controller is -4.84 rad/s compared to -1.48 rad/s of contact-aware policy which also demonstrates that contact-aware policy is reacting better to the falling pole as expected.

We examine a specific trial (see Fig. 21), where the differences between the preimpact states are 0.01, 0.02, 0.2, and 0.01 for x_1, x_2, x_3, x_4, respectively. Over the 50 ms impact period, change in the cart velocity with contact-aware controller is 2.2 m/s higher than LQR. Similarly, the change in angular velocity of the pole is 3.01 rd/s more than LQR. As shown in Fig. 21, as soon as the impact event with the left wall starts the contact-aware policy tries to push the cart in the positive direction in order to catch the falling pole and stabilizes the system unlike LQR.

Experiment 2. In the first experiment, we created a consistent initial condition across all trials. Here, we introduce random perturbations to cover a broader range of initial conditions. As with the first experiment, the goal of the initialization process is to create conditions which initiate contact. First, the system is balanced at the origin. Then, we apply a control input[8] briefly to ensure that pole is close to impacting the left wall with a relatively high speed. Next, we apply a random input disturbance with uniform distribution $u_d \sim U[5, 10]$ for 100 ms. We repeat this experiment 10 times for each LQR and contact-aware policy (with same seeds). After the random input disturbance is applied, the states are distributed as shown in Fig. 22.

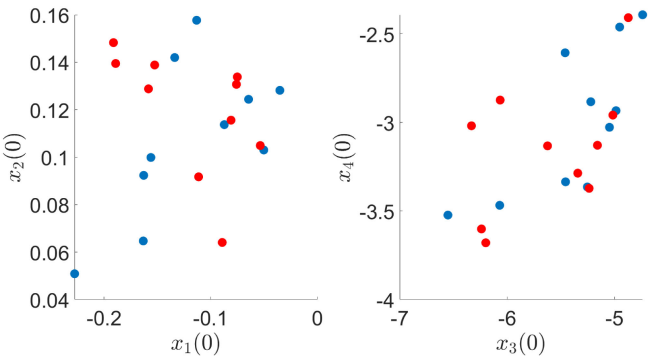

Fig. 22. Experiment 2—Distribution of initial conditions where blue represents contact-aware policy trials and red represents LQR trials.

Out of the ten trials, the LQR controller failed in 5/10 of the trials, whereas the contact-aware policy was always successful. In Fig. 23, we demonstrate that the contact-aware policy ends up with a lower cost-to-go than LQR after the impact event. Note that LQR cost-to-go is a useful metric, more so than the two-norm, since it represents an approximate cost to complete the stabilization task.

Experiment 3. After the impact event, the walls oscillate back and forth, which causes oscillations in sensor readings as shown in Fig. 24. In this experiment, we do not apply a threshold to the sensor readings. This enables pure feedback on sensor measurements, rather than heuristic-based thresholds or slow/inaccurate mode detection (where the state-of-the-art takes 4–5 ms [68]) that purely hybrid approaches utilize. Hence, we repeat the procedure in Experiment 1 and observe that the controller is

[8]We apply the control input $u = K(x - x_s)$, where $x_s^T = \begin{bmatrix} 0 & 0.5 & 0 & 0 \end{bmatrix}$ for 0.5 seconds and switch back to $x_s^T = \begin{bmatrix} 0 & 0 & 0 & 0 \end{bmatrix}$.

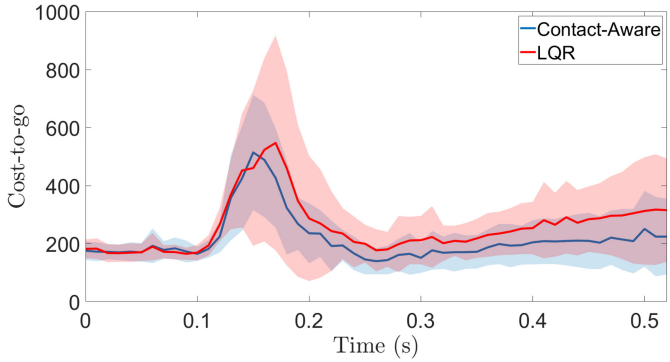

Fig. 23. Experiment 2—LQR cost-to-go for all trials during the impact event (impact events are aligned for all trials). Blue represents contact-aware policy, red represents LQR, solid lines represent the respective means and shaded regions represent standard deviation. Contact-aware cost-to-go surpasses LQR cost-to-go as the impact starts due to the aggressive tactile feedback but contact-aware policy ends up with a lower cost-to-go after the impact event.

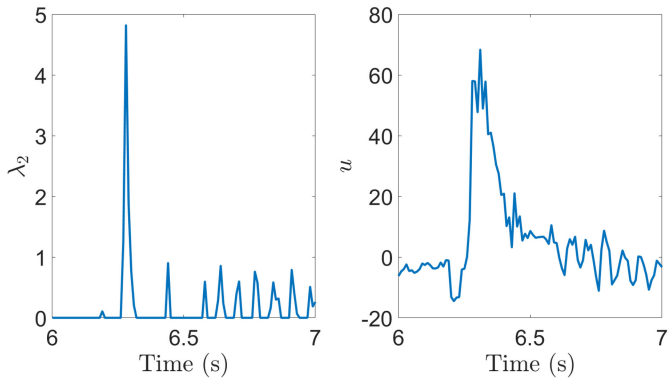

Fig. 24. Experiment 3—The oscillations in sensor readings (λ_2) that are caused by the impact event and the corresponding control action without heuristic-based thresholds.

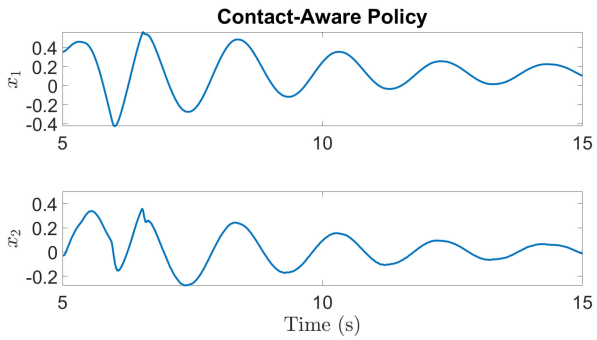

Fig. 25. Experiment 3—Trajectory with contact-aware controller without any heuristic-based thresholds.

successful in stabilizing the system (see Fig. 25) even without heuristic-based thresholds. In Fig. 26, model is simulated (as in Section VI-A) starting from the an initial condition obtained from the experiment and contact-aware policy stabilizes the system, whereas LQR fails. This demonstrates that simulations capture the system qualitatively.

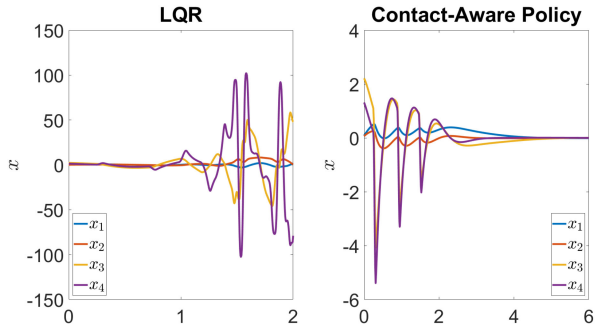

Fig. 26. Experiment 3—Simulation results (as in Section VI-A) where we simulate forward from a state obtained from the experiment. Simulation captures the system response qualitatively as LQR is unstable and contact-aware policy is successful.

VIII. Conclusion

In this work, we introduced a controller that can utilize both state and force feedback. We demonstrated that combining LCSs with such tactile feedback controllers might result in an algebraic loop, and discussed how one can break such algebraic loops.

We proposed an algorithm for synthesizing contact-aware control policies for LCSs with possibly nonunique solutions. For soft contact models, we have shown that pure local, linear analysis was entirely insufficient and utilizing contact in the control design is critical to achieve high performance. For systems with nonunique solutions, we have proposed a polynomial optimization program that can find matrices that map nonunique contact forces into a unique value, and used such mappings in our controller design algorithm. We have shown the effectiveness of our method on quasi-static friction models.

Furthermore, the proposed algorithm exploits the complementarity structure of the system and avoids enumerating the exponential number of potential modes, enabling efficient design of multicontact control policies. Toward this direction, we have presented an example with eight states and ten contacts. In addition to incorporating tactile sensing into dynamic feedback, we provide stability guarantees for our design method and we have verified our method on an experimental setup.

The algorithm requires solving feasibility problems that include BMIs and we have used PENBMI [62]. For the examples presented here, except the last one, the runtime of the algorithm was short and we found solutions to the problems relatively quickly. On the other hand, it is important to note that for some parameter choices and initializations, the solver was unable to produce feasible solutions.

Interesting future work in this area will be using the controller presented here in physical experiments. We consider a hierarchical control framework, where the tactile feedback policy is the higher level controller working together with a lower level controller to achieve a specified task. In addition, we intend to extend these algorithms to more complex tasks. For example, quasi-static models [23], where the matrix F depends on the generalized coordinates q. Another direction is designing controllers for systems, where there are bilinear terms $(x_i\lambda_j)$ in the dynamics, since we believe that bilinear terms are important when locally approximating a certain class of

nonsmooth systems. Also, works such as [24] draw connections between compliant and rigid contact models. Such approaches can help analyzing the controllers designed in this work for a range wider range of models. Last, it may be possible to increase the application of our method by utilizing nonmonotonic and almost-decreasing Lyapunov functions [36].

APPENDIX A

Next, we present the matrix inequalities in (15) and (16) explicitly. We can represent (15) as follows:

$$T_1 - S_1^T W_1 S_1 - \frac{1}{2}(S_{2,1} + S_{2,1}^T) \succeq 0$$
$$T_2 + S_1^T W_2 S_1 + \frac{1}{2}(S_{2,2} + S_{2,2}^T) \preceq 0$$

where W_i are decision variables with nonnegative entries, $J_i = \text{diag}(\tau_i)$, where τ_i are free decision variables, and

$$T_1 = \begin{bmatrix} P - \gamma_1 I & Q & p/2 \\ * & R & r/2 \\ * & * & z \end{bmatrix}, T_2 = \begin{bmatrix} P - \gamma_2 I & Q & p/2 \\ * & R & r/2 \\ * & * & z \end{bmatrix}$$
$$S_1 = \begin{bmatrix} E & F & c \\ 0 & I & 0 \\ 0 & 0 & 1 \end{bmatrix}, S_{2,i} = \begin{bmatrix} 0 & 0 & 0 \\ J_i E & J_i F & J_i c \\ 0 & 0 & 0 \end{bmatrix}.$$

We can represent (15) as follows:

$$T_3 + S_3^T W_3 S_3 + \frac{1}{2}(S_4 + S_4^T) + \sum_{i=1}^{m} \frac{1}{2}(S_{5,i} + S_{5,i}^T) \preceq 0$$

where W_i are decision variables with nonnegative entries, $J_i = \text{diag}(\tau_i)$, where τ_i are free decision variables and $\zeta_{5,i} = \text{diag}(\theta_i)$, where θ_i are zero everywhere expect the ith entry which is a free variable and (T_3 is symmetric)

$$T_3 = \begin{bmatrix} PA + A^T P & PD + A^T Q & Q & A^T p/2 + Pa & 0 & 0 \\ * & D^T Q + Q^T D & R & Q^T a + D^T p/2 & 0 & 0 \\ * & * & 0 & r/2 & 0 & 0 \\ * & * & * & p^T a & 0 & 0 \\ 0 & 0 & 0 & 0 & 0 & 0 \\ 0 & 0 & 0 & 0 & 0 & 0 \end{bmatrix}$$

$$S_3 = \begin{bmatrix} E & F & 0 & c & 0 & 0 \\ 0 & I & 0 & 0 & 0 & 0 \\ 0 & 0 & 0 & 1 & 0 & 0, \end{bmatrix}$$

$$S_4 = \begin{bmatrix} 0 & 0 & 0 & 0 & 0 & 0 \\ J_3 E & J_3 F & 0 & J_3 c & 0 & 0 \\ 0 & 0 & 0 & 0 & 0 & 0 \\ J_4 E A & J_4 E D & J_4 F + J_5 & J_4 E a & J_4 & J_5 \\ 0 & 0 & 0 & 0 & 0 & 0 \\ 0 & 0 & 0 & 0 & 0 & 0 \end{bmatrix}$$

$$S_{5,i} = \begin{bmatrix} 0 & 0 & 0 & 0 & 0 & 0 \\ 0 & 0 & 0 & 0 & \zeta_{7,i} & 0 \\ 0 & 0 & 0 & 0 & 0 & 0 \\ 0 & 0 & 0 & 0 & 0 & 0 \\ 0 & 0 & 0 & 0 & 0 & \zeta_{8,i} \\ \zeta_{9,i} E & \zeta_{9,i} F & 0 & \zeta_{9,i} c & 0 & 0 \end{bmatrix}.$$

APPENDIX B

We present the two polynomial optimization problems. The first one is regarding Proposition 15:

$$\begin{aligned} \text{find} \quad & w, \eta, p_i^k, p_{i,j}^k, s_i^k \\ \text{subject to} \quad & \phi_1(\boldsymbol{\lambda}_1, \boldsymbol{\lambda}_2, \boldsymbol{q}) \geq 0 \\ & \phi_2(\boldsymbol{\lambda}_1, \boldsymbol{\lambda}_2, \boldsymbol{q}) \geq 0 \end{aligned} \tag{39}$$

and the second one considers the optimization problem in (27)

$$\begin{aligned} \min_{w, \eta, p_i^k, p_{i,j}^k, s_i^k} \quad & r^T N^T w \\ \text{subject to} \quad & \phi_1(\boldsymbol{\lambda}_1, \boldsymbol{\lambda}_2, \boldsymbol{q}) \geq 0 \\ & \phi_2(\boldsymbol{\lambda}_1, \boldsymbol{\lambda}_2, \boldsymbol{q}) \geq 0 \\ & |w_i| \leq 1, \ \forall i, \ \eta \geq 0 \end{aligned} \tag{40}$$

where the functions ϕ_1 and ϕ_2 are defined as

$$\begin{aligned} \phi_1(\boldsymbol{\lambda}_1, \boldsymbol{\lambda}_2, \boldsymbol{q}) = & (\eta + w^T(\boldsymbol{\lambda}_1 - \boldsymbol{\lambda}_2))(\boldsymbol{\lambda}_1^T \boldsymbol{\lambda}_1 + \boldsymbol{\lambda}_2^T \boldsymbol{\lambda}_2) \\ & + \sum_i p_i^1 \boldsymbol{\lambda}_{1,i} + \sum_i p_i^2 \boldsymbol{\lambda}_{2,i} + \sum_i \sum_j p_{i,j}^3 \boldsymbol{\lambda}_{1,i} \boldsymbol{\lambda}_{1,j} \\ & + \sum_i p_i^4 (\boldsymbol{q}_i + F_i^T \boldsymbol{\lambda}_1) + \sum_i p_i^5 (\boldsymbol{q}_i + F_i^T \boldsymbol{\lambda}_2) \\ & + \sum_i \sum_j p_{i,j}^6 (\boldsymbol{q}_i + F_i^T \boldsymbol{\lambda}_1)(\boldsymbol{q}_j + F_j^T \boldsymbol{\lambda}_2) \\ & + \sum_i \sum_j p_{i,j}^7 (\boldsymbol{q}_i + F_i^T \boldsymbol{\lambda}_2) \boldsymbol{\lambda}_{1,j} \\ & + \sum_i \sum_j p_{i,j}^8 (\boldsymbol{q}_i + F_i^T \boldsymbol{\lambda}_1) \boldsymbol{\lambda}_{2,j} \\ & + \sum_i s_i^1 \boldsymbol{\lambda}_{1,i} (\boldsymbol{q}_i + F_i^T \boldsymbol{\lambda}_1) \\ & + \sum_i s_i^2 \boldsymbol{\lambda}_{2,i} (\boldsymbol{q}_i + F_i^T \boldsymbol{\lambda}_2) \end{aligned}$$

where $p_i^k, p_{i,j}^k$ are nonnegative variables (SOS polynomials), s_i^k are free variables (polynomials with no restriction) and

$$\begin{aligned} \phi_2(\boldsymbol{\lambda}_1, \boldsymbol{\lambda}_2, \boldsymbol{q}) = & (\eta - w^T(\boldsymbol{\lambda}_1 - \boldsymbol{\lambda}_2))(\boldsymbol{\lambda}_1^T \boldsymbol{\lambda}_1 + \boldsymbol{\lambda}_2^T \boldsymbol{\lambda}_2) \\ & + \sum_i p_i^9 \boldsymbol{\lambda}_{1,i} + \sum_i p_i^{10} \boldsymbol{\lambda}_{2,i} + \sum_i \sum_j p_{i,j}^{11} \boldsymbol{\lambda}_{1,i} \boldsymbol{\lambda}_{1,j} \\ & + \sum_i p_i^{12} (\boldsymbol{q}_i + F_i^T \boldsymbol{\lambda}_1) + \sum_i p_i^{13} (\boldsymbol{q}_i + F_i^T \boldsymbol{\lambda}_2) \end{aligned}$$

$$+\sum_i\sum_j p_{i,j}^{14}(\boldsymbol{q}_i+F_i^T\boldsymbol{\lambda}_1)(\boldsymbol{q}_j+F_j^T\boldsymbol{\lambda}_2)$$

$$+\sum_i\sum_j p_{i,j}^{15}(\boldsymbol{q}_i+F_i^T\boldsymbol{\lambda}_2)\boldsymbol{\lambda}_{1,j}$$

$$+\sum_i\sum_j p_{i,j}^{16}(\boldsymbol{q}_i+F_i^T\boldsymbol{\lambda}_1)\boldsymbol{\lambda}_{2,j}$$

$$+\sum_i s_i^3\boldsymbol{\lambda}_{1,i}(\boldsymbol{q}_i+F_i^T\boldsymbol{\lambda}_1)$$

$$+\sum_i s_i^4\boldsymbol{\lambda}_{2,i}(\boldsymbol{q}_i+F_i^T\boldsymbol{\lambda}_2)$$

where $p_i^k, p_{i,j}^k$ are nonnegative variables (SOS polynomials), s_i^k are free variables (polynomials with no restriction).

ACKNOWLEDGMENT

The authors would like to thank the reviewers, who have offered many constructive comments that have significantly improved this article. The authors also like to thank Brian Acosta, William Yang, and Yu-Ming Chen for their help with the experimental setup.

REFERENCES

[1] J. K. Mills and D. M. Lokhorst, "Control of robotic manipulators during general task execution: A discontinuous control approach," *Int. J. Robot. Res.*, vol. 12, no. 2, pp. 146–163, 1993.

[2] J. K. Mills and D. M. Lokhorst, "Stability and control of robotic manipulators during contact/noncontact task transition," *IEEE Trans. Robot. Automat.*, vol. 9, no. 3, pp. 335–345, Jun. 1993.

[3] C. Mastalli *et al.*, "Crocoddyl: An efficient and versatile framework for multi-contact optimal control," in *Proc. IEEE Int. Conf. Robot. Automat.*, 2020, pp. 2536–2542.

[4] A. W. Winkler, C. D. Bellicoso, M. Hutter, and J. Buchli, "Gait and trajectory optimization for legged systems through phase-based end-effector parameterization," *IEEE Robot. Automat. Lett.*, vol. 3, no. 3, pp. 1560–1567, Jul. 2018.

[5] Y. Tassa, T. Erez, and E. Todorov, "Synthesis and stabilization of complex behaviors through online trajectory optimization," in *Proc. IEEE/RSJ Int. Conf. Intell. Robots Syst.*, 2012, pp. 4906–4913.

[6] F. R. Hogan, E. R. Grau, and A. Rodriguez, "Reactive planar manipulation with convex hybrid MPC," in *Proc. IEEE Int. Conf. Robot. Automat.*, 2018, pp. 247–253.

[7] T. Marcucci and R. Tedrake, "Warm start of mixed-integer programs for model predictive control of hybrid systems," *IEEE Trans. Automat. Control*, vol. 66, no. 6, pp. 2433–2448, Jun. 2021.

[8] M. Posa, M. Tobenkin, and R. Tedrake, "Stability analysis and control of rigid-body systems with impacts and friction," *IEEE Trans. Autom. Control*, vol. 61, no. 6, pp. 1423–1437, Jun. 2016.

[9] N. Wettels, J. Fishel, Z. Su, C. Lin, and G. Loeb, "Multi-modal synergistic tactile sensing," in *Proc. Tactile Sens. Humanoids–Tactile Sensors Beyond Workshop, 9th IEEE-RAS Int. Conf. Humanoid Robots*, 2009, pp. 1–3.

[10] J. W. Guggenheim, L. P. Jentoft, Y. Tenzer, and R. D. Howe, "Robust and inexpensive six-axis force-torque sensors using MEMS barometers," *IEEE/ASME Trans. Mechatronics*, vol. 22, no. 2, pp. 838–844, Apr. 2017.

[11] W. Yuan, R. Li, M. A. Srinivasan, and E. H. Adelson, "Measurement of shear and slip with a GelSight tactile sensor," in *Proc. IEEE Int. Conf. Robot. Automat.*, 2015, pp. 304–311.

[12] V. Kumar, E. Todorov, and S. Levine, "Optimal control with learned local models: Application to dexterous manipulation," in *Proc. IEEE Int. Conf. Robot. Automat.*, 2016, pp. 378–383.

[13] E. Donlon, S. Dong, M. Liu, J. Li, E. Adelson, and A. Rodriguez, "GelSlim: A high-resolution, compact, robust, and calibrated tactile-sensing finger," in *Proc. IEEE/RSJ Int. Conf. Intell. Robots Syst.*, 2018, pp. 1927–1934.

[14] R. D. Howe, "Tactile sensing and control of robotic manipulation," *Adv. Robot.*, vol. 8, no. 3, pp. 245–261, 1993.

[15] J. M. Romano, K. Hsiao, G. Niemeyer, S. Chitta, and K. J. Kuchenbecker, "Human-inspired robotic grasp control with tactile sensing," *IEEE Trans. Robot.*, vol. 27, no. 6, pp. 1067–1079, Dec. 2011.

[16] A. Yamaguchi and C. G. Atkeson, "Combining finger vision and optical tactile sensing: Reducing and handling errors while cutting vegetables," in *Proc. IEEE-RAS 16th Int. Conf. Humanoid Robots (Humanoids)*, 2016, pp. 1045–1051.

[17] H. Merzic, M. Bogdanovic, D. Kappler, L. Righetti, and J. Bohg, "Leveraging contact forces for learning to grasp," in *Proc. Int. Conf. Robot. Automat.*, 2018, pp. 3615–3621.

[18] S. Tian *et al.*, "Manipulation by feel: Touch-based control with deep predictive models," in *Proc. Int. Conf. Robot. Automat.*, 2019, pp. 818–824.

[19] M. Camlibel *et al.*, "Complementarity methods in the analysis of piecewise linear dynamical systems," Ph.D. dissertation, School Econ. Manage., Tilburg Univ., 2001.

[20] A. Aydinoglu, V. M. Preciado, and M. Posa, "Contact-aware controller design for complementarity systems," in *Proc. IEEE Int. Conf. Robot. Automat.*, 2019, pp. 1525–1531.

[21] R. Alur, T. A. Henzinger, G. Lafferriere, and G. J. Pappas, "Discrete abstractions of hybrid systems," *Proc. IEEE Proc. IRE*, vol. 88, no. 7, pp. 971–984, Jul. 2000.

[22] M. S. Branicky, V. S. Borkar, and S. K. Mitter, "A unified framework for hybrid control: Model and optimal control theory," *IEEE Trans. Autom. Control*, vol. 43, no. 1, pp. 31–45, Jan. 1998.

[23] M. Halm and M. Posa, "A quasi-static model and simulation approach for pushing, grasping, and jamming," in *Proc. Int. Workshop Algorithmic Found. Robot.*, 2019, pp. 491–507.

[24] B. Brogliato, *Nonsmooth Mechanics: Models, Dynamics and Control*. Berlin, Germany: Springer, 2016.

[25] D. E. Stewart, "Rigid-body dynamics with friction and impact," *SIAM Rev.*, vol. 42, no. 1, pp. 3–39, 2000.

[26] R. I. Leine and N. V. de Wouw, *Stability and Convergence of Mechanical Systems With Unilateral Constraints*, vol. 36. Berlin, Germany: Springer, 2007.

[27] M. Anitescu and F. A. Potra, "Formulating dynamic multi- contact problems with friction as solvable linear complementarity problems," *Nonlinear Dyn.*, vol. 14, no. 3, pp. 231–247, 1997.

[28] D. Stewart and J. C. Trinkle, "An Implicit Time-Stepping Scheme for Rigid Body Dynamics With Coulomb Friction," in *Proc. IEEE Int. Conf. Robot. Automat. Symposia (Cat. No 00CH37065)*, 2000, vol. 1, pp. 162–169.

[29] M. Posa, C. Cantu, and R. Tedrake, "A direct method for trajectory optimization of rigid bodies through contact," *Int. J. Robot. Res.*, vol. 33, no. 1, pp. 69–81, 2014.

[30] M. Haas-Heger, G. Iyengar, and M. Ciocarlie, "On the distinction between active and passive reaction in grasp stability analysis," in *Proc. Workshop Algorithmic Found. Robot.*, 2016, pp. 448–463.

[31] B. Brogliato, R. Lozano, B. Maschke, and O. Egeland, "Dissipative systems analysis and control," *Theory Appl.*, vol. 2, pp. 357–451, 2007.

[32] A. Zavala-Rio and B. Brogliato, "Direct adaptive control design for one-degree-of-freedom complementary-slackness jugglers," *Automatica*, vol. 37, no. 7, pp. 1117–1123, 2001.

[33] C.-I. Morărescu and B. Brogliato, "Passivity-based switching control of flexible-joint complementarity mechanical systems," *Automatica*, vol. 46, no. 1, pp. 160–166, 2010.

[34] M. K. Çamlıbel, W. Heemels, and J. Schumacher, "On linear passive complementarity systems," *Eur. J. Control*, vol. 8, no. 3, pp. 220–237, 2002.

[35] L. Menini and A. Tornambé, "Velocity observers for non-linear mechanical systems subject to non-smooth impacts," *Automatica*, vol. 38, no. 12, pp. 2169–2175, 2002.

[36] I. C. Morrescu and B. Brogliato, "Trajectory tracking control of multiconstraint complementarity Lagrangian systems," *IEEE Trans. Autom. Control*, vol. 55, no. 6, pp. 1300–1313, Jun. 2010.

[37] L. Menini and A. Tornambé, "Asymptotic tracking of periodic trajectories for a simple mechanical system subject to nonsmooth impacts," *IEEE Trans. Autom. Control*, vol. 46, no. 7, pp. 1122–1126, Jul. 2001.

[38] B. Brogliato, "Feedback control of multibody systems with joint clearance and dynamic backlash: A tutorial," *Multibody Syst. Dyn.*, vol. 42, no. 3, pp. 283–315, 2018.

[39] B. Brogliato and A. Z. Rio, "On the control of complementary-slackness juggling mechanical systems," *IEEE Trans. Autom. Control*, vol. 45, no. 2, pp. 235–246, Feb. 2000.

[40] B. Brogliato, S.-I. Niculescu, and P. Orhant, "On the control of finite-dimensional mechanical systems with unilateral constraints," *IEEE Trans. Autom. Control*, vol. 42, no. 2, pp. 200–215, Feb. 1997.

[41] W. Heemels, J. M. Schumacher, and S. Weiland, "Linear complementarity systems," *SIAM J. Appl. Math.*, vol. 60, no. 4, pp. 1234–1269, 2000.
[42] D. Q. Mayne, "Control of constrained dynamic systems," *Eur. J. Control*, vol. 7, no. 2-3, pp. 87–99, 2001.
[43] H. Lin and P. J. Antsaklis, "Stability and stabilizability of switched linear systems: A survey of recent results," *IEEE Trans. Autom. Control*, vol. 54, no. 2, pp. 308–322, Feb. 2009.
[44] R. W. Cottle, J.-S. Pang, and R. E. Stone, *The Linear Complementarity Problem*. Philadelphia, PA, USA: SIAM, 2009.
[45] J. Shen and J.-S. Pang, "Linear complementarity systems: Zeno states," *SIAM J. Control Optim.*, vol. 44, no. 3, pp. 1040–1066, 2005.
[46] P. A. Parrilo, "Semidefinite programming relaxations for semialgebraic problems," *Math. Program.*, vol. 96, no. 2, pp. 293–320, 2003.
[47] G. Stengle, A. Nullstellensatz, and A. Positivstellensatz. "In Semialgebraic Geometry,"," *Mathematische Annalen*, vol. 207, no. 2, pp. 87–97, 1974.
[48] S. Boyd, L. E. Ghaoui, E. Feron, and V. Balakrishnan, *Linear Matrix Inequalities in System and Control Theory*, vol. 15. Philadelphia, PA, USA: SIAM, 1994.
[49] M. A. Posa, T. Koolen, and R. L. Tedrake, "Balancing and step recovery capturability via sums-of-squares optimization," 2017.
[50] M. Çamlibel, W. Heemels, A. van der Schaft, and J. Schumacher, "Solution concepts for hybrid dynamical systems," in *Proc. IFAC World Congr.*, 2002, pp. 1217–1222.
[51] J. Shen and J.-S. Pang, "Semicopositive linear complementarity systems," *Int. J. Robust Nonlinear Control, IFAC-Affiliated J.*, vol. 17, no. 15, pp. 1367–1386, 2007.
[52] B. Brogliato and L. Thibault, "Existence and uniqueness of solutions for non-autonomous complementarity dynamical systems," *J. Convex Anal.*, vol. 17, no. 3–4, pp. 961–990, 2010.
[53] M. K. Camlibel, J.-S. Pang, and J. Shen, "Lyapunov stability of complementarity and extended systems," *SIAM J. Optim.*, vol. 17, no. 4, pp. 1056–1101, 2006.
[54] B. Brogliato and A. Tanwani, "Dynamical systems coupled with monotone set-valued operators: Formalisms, applications, well-posedness, and stability," *SIAM Rev.*, vol. 62, no. 1, pp. 3–129, 2020.
[55] G. V. Smirnov, *Introduction to the Theory of Differential Inclusions*, vol. 41. Providence, Rhode Island, USA: Amer. Math. Soc., 2002.
[56] H. K. Khalil, *Nonlinear Systems*. Upper Saddle River, NJ, USA: Prentice Hall, 2002.
[57] M. Johansson and A. Rantzer, "Computation of piecewise quadratic Lyapunov functions for hybrid systems," in *Proc. Eur. Control Conf.*, 1997, pp. 2005–2010.
[58] A. Papachristodoulou and S. Prajna, "Robust stability analysis of nonlinear hybrid systems," *IEEE Trans. Autom. Control*, vol. 54, pp. 1035–1041, May 2009.
[59] MOSEK ApS, "The MOSEK optimization toolbox for MATLAB manual," Version 9.0, 2019. [Online]. Available: http://docs.mosek.com/9.0/toolbox/index.html
[60] J. F. Sturm, "Using SeDuMi 1.02, A MATLAB toolbox for optimization over symmetric cones," *Optim. Methods Softw.*, vol. 11, no. 1–4, pp. 625–653, 1999.
[61] J. Löfberg, "YALMIP : A toolbox for modeling and optimization in MATLAB," in *Proc. Symp. Comput. Aided Control Syst. Des. Conf.*, Taipei, Taiwan, 2004, pp. 284–289.
[62] M. Kočvara and M. Stingl, "PENNON: A code for convex nonlinear and semidefinite programming," *Optim. Methods Softw.*, vol. 18, no. 3, pp. 317–333, 2003.
[63] S. P. Dirkse and M. C. Ferris, "The PATH solver: A non-monotone stabilization scheme for mixed complementarity problems," *Optim. Methods Softw.*, vol. 5, no. 2, pp. 123–156, 1995.
[64] R. Deits, T. Koolen, and R. Tedrake, "LVIS: Learning from value function intervals for contact-aware robot controllers," in *Proc. Int. Conf. Robot. Automat.*, 2019, pp. 7762–7768.
[65] T. Marcucci, R. Deits, M. Gabiccini, A. Bicchi, and R. Tedrake, "Approximate hybrid model predictive control for multi-contact push recovery in complex environments," in *Proc. IEEE-RAS 17th Int. Conf. Humanoid Robot. (Humanoids)*, 2017, pp. 31–38.
[66] B. Brogliato, "Some perspectives on the analysis and control of complementarity systems," *IEEE Trans. Autom. Control*, vol. 48, no. 6, pp. 918–935, Jun. 2003.
[67] R. M. Murray and J. E. Hauser, *A Case Study in Approximate Linearization: The Acrobat Example*, Electronics Research Laboratory, College of Engineering, University of California, 1991.
[68] G. Bledt, M. J. Powell, B. Katz, J. Di Carlo, P. M. Wensing, and S. Kim, "MIT Cheetah 3: Design and control of a robust, dynamic quadruped robot," in *Proc. IEEE/RSJ Int. Conf. Intell. Robots Syst.*, 2018, pp. 2245–2252.

Alp Aydinoglu (Graduate Student Member, IEEE) received the B.S. degree in control engineering from Istanbul Technical University, Istanbul, Turkey, in 2017. He is currently working toward the Ph.D. degree in electrical and systems engineering with the University of Pennsylvania, Philadelphia, PA, USA.

He is currently working with Michael Posa in Dynamic Autonomy and Intelligent Robotics (DAIR) Lab. His research emphasizes control of multicontact systems.

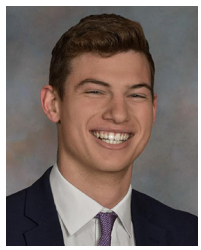

Philip Sieg is currently working toward the B.Eng. degree in mechanical engineering and the MSE degree in robotics from the University of Pennsylvania. Philadelphia, PA, USA.

His research interests include hardware design for robotics, legged locomotion, mobile robots, and grasping.

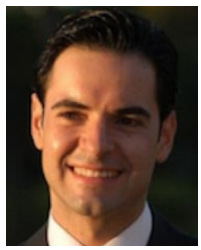

Victor M. Preciado (Senior Member, IEEE) received the Ph.D. degree in electrical engineering and computer science from the Massachusetts Institute of Technology, Cambridge, MA, USA, in 2008.

He is currently an Associate Professor and Graduate Chair with the Department of Electrical and Systems Engineering, University of Pennsylvania, where he is affiliated with the Networked and Social Systems Engineering program, the Warren Center for Network and Data Sciences, and the Applied Math and Computational Science program. He was a Postdoctoral Researcher with the GRASP lab.

Prof. Preciado was a recipient of the 2017 National Science Foundation CAREER Award, the 2018 Best Paper Award by the IEEE CONTROL SYSTEMS MAGAZINE, and a runner-up of the 2019 Best Paper Award by the IEEE TRANSACTIONS ON NETWORK SCIENCE AND ENGINEERING. He is an Associate Editor of the IEEE TRANSACTIONS ON NETWORK SCIENCE AND ENGINEERING and the IEEE TRANSACTIONS ON CONTROL OF NETWORKED SYSTEMS.

Michael Posa (Member, IEEE) received the Ph.D. degree in electrical engineering and computer science from the Massachusetts Institute of Technology, Cambridge, MA, USA, in 2017.

He is currently an Assistant Professor of mechanical engineering and applied mechanics with the University of Pennsylvania, where he is a member of the General Robotics, Automation, Sensing and Perception (GRASP) Lab. He holds secondary appointments in electrical and systems engineering and in computer and information science. He leads to Dynamic Autonomy and Intelligent Robotics (DAIR) Lab, which focuses on developing computationally tractable algorithms to enable robots to operate both dynamically and safely as they maneuver through and interact with their environments, with applications including legged locomotion and manipulation.

Prof. Posa was a recipient of the best paper award at Hybrid Systems: Computation and Control, a Google Faculty Research Award, and the Young Faculty Researcher award from the Toyota Research Institute. He is an Associate Editor for the IEEE ROBOTICS AND AUTOMATION LETTERS.